FINAL REPORT OF

SURFACE BRIGHTNESS MEASUREMENTS OF SUPERNOVA REMNANTS IN THE ENERGY BAND 0.15 - 4 keV AND AN XUV SURVEY FROM AN ATTITUDE CONTROLLED ROCKET

CALIFORNIA INSTITUTE OF TECHNOLOGY

PASADENA, CALIFORNIA

CALIFORNIA INSTITUTE OF TECHNOLOGY

DIVISION OF PHYSICS, MATHEMATICS, AND ASTRONOMY

PASADENA, CALIFORNIA

FINAL REPORT TO THE

NATIONAL AERONAUTICS AND SPACE ADMINISTRATION

FINAL REPORT OF

SURFACE BRIGHTNESS MEASUREMENTS OF SUPERNOVA REMNANTS IN THE ENERGY BAND 0.15 - 4 keV AND AN XUV SURVEY FROM AN ATTITUDE CONTROLLED ROCKET

NASA GRANT NGR 05002219

EFFECTIVE: 1 MAY 1971 - 31 MARCH 1973

Submitted by:

Gordon P. Garmire
Principal Investigator

Guenter Riegler
Co-Investigator

The enclosed papers are submitted to constitute the final report on the flight of Aerobee 170, 13.063 UG. The flight was quite successful and provided all of the information that was anticipated. A photograph of the payload is included for reference purposes. The upper bank of detectors form the mapping experiment and the lower bank constitute the spectral experiment. The XUV telescope is adjacent to the aspect camera near the midpoint of the experiment.

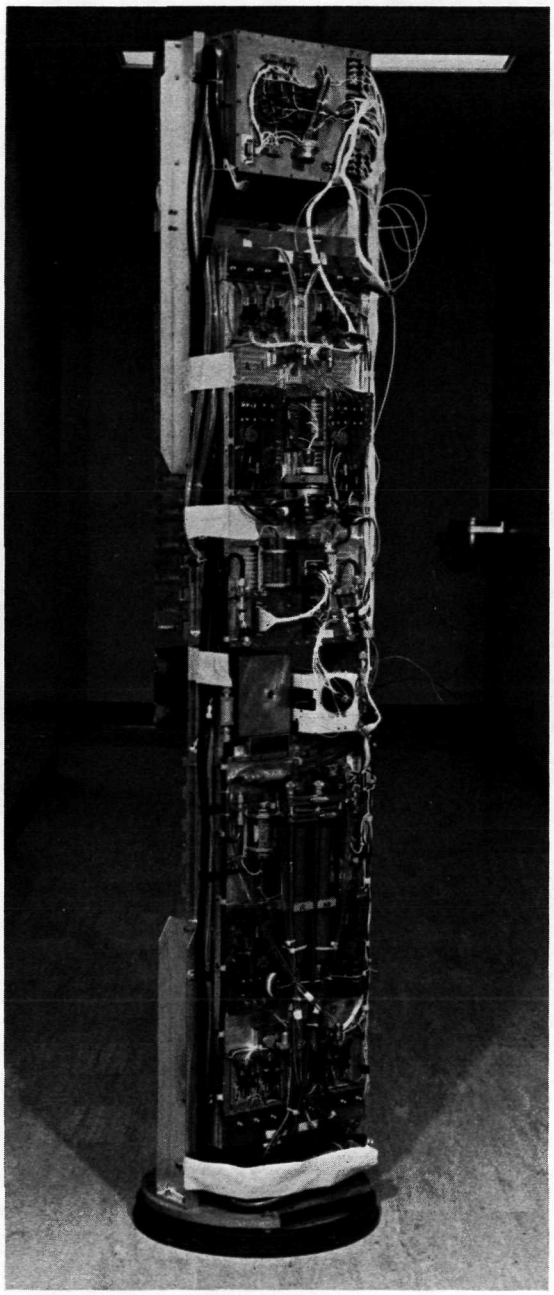

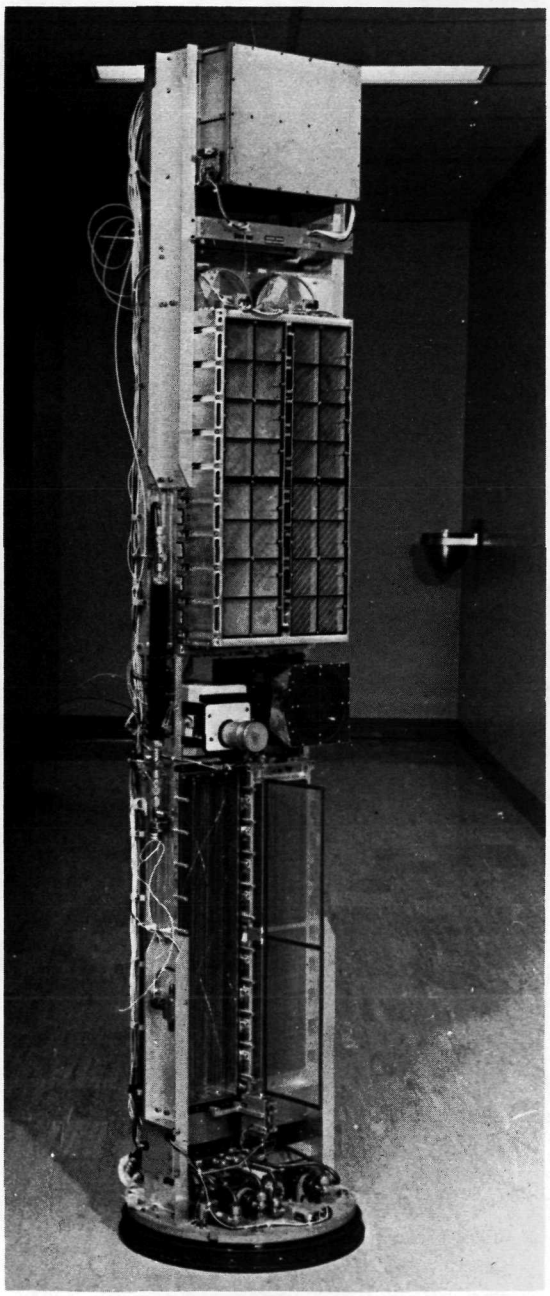

THE ASTROPHYSICAL JOURNAL, 175:L73–L77, 1972 July 15

SOFT X-RAYS FROM CYGNUS X-2 AND FROM CYGNUS X-1 (IN ECLIPSE?)

J. C. STEVENS, G. P. GARMIRE, AND G. R. RIEGLER*
Division of Physics, Mathematics and Astronomy, California Institute of Technology
Received 1972 April 28

ABSTRACT

Cygnus X-1 and Cygnus X-2 were observed on 1971 October 23. The intensity of Cyg X-1 was in a low state at the time of observation which corresponded to the time of possible eclipse of the companion of BD+34°3815 (HDE 226868). The intensity of Cyg X-2 was measured to be comparable to previous observations, with an interstellar cutoff corresponding to $0.8 \pm 0.4 \times 10^{21}$ H atoms per cm^2.

I. INTRODUCTION

On 1971 October 23 at 03^h47^m UT Cyg X-1 and Cyg X-2 were observed in the energy band 0.2–2.5 keV by an experiment on an Aerobee 170 launched from the White Sands Missile Range, New Mexico. At the time of the observation the star BD+34°3815, the optical candidate for Cyg X-1, was potentially occulting its unseen companion in this binary system. The flux received from Cyg X-1 at this time is quite low compared to other reported flux levels.

II. INSTRUMENTATION

The detectors were composed of four banks of multilayer and multiwire proportional counters filled to 150 torr with pure methane gas. The window of one detector was a 1.5-μ polypropylene plastic film, and a second detector was covered by two such films. The open area of each of these two detectors was about 400 cm^2 and the collimation was achieved by using slat collimators with fields of view of about $11° \times 11°$. The two other detectors were covered with 2-μ Kimfol and collimated to $0°.4 \times 10°$. They did not obtain a sufficient number of counts during the transit of Cyg X-1 for spectral studies. A more complete description of the instrument is given by Garmire and Riegler (1972).

The two large-field-of-view detectors observed Cyg X-1 with significant sensitivity for about 6 s during the flight. The attitude of the detectors was determined by star-field photographs taken once each second, to a precision of about 20′ during the scan near Cyg X-1. Calibration sources mounted on the door of the rocket provided a check on the gain and resolution of the detectors just prior to the observation and at the end of the flight. No change in gain during the flight was observed within the calibration accuracy of 5 percent. The linearity of the detector system was checked carefully at six energies before flight using ^{210}Po activated fluorescence sources. The overall system did not deviate from linearity by more than 2 percent at any measured energy between 0.28 and 2.3 keV.

III. OBSERVATIONS

The observation of Cyg X-1 is shown in figure 1, compared to a recent report by Schreier *et al.* (1971). Observations by Overbeck and Tananbaum (1968), Haymes and Harnden (1970), and Webber and Reinert (1970) are shown for comparison. It is interesting to note that an extrapolation of the balloon observations nearly fits the data reported here. The low-energy portion of our data is contaminated with a small fraction of the flux from the Cygnus Loop which passed within about 9° of the center of the collimator field of view during the Cyg X-1 transit. Later in the flight the spectrum of the

* Present address: Bendix Corporation, 3300 Plymouth Road, Ann Arbor, Michigan 48105.

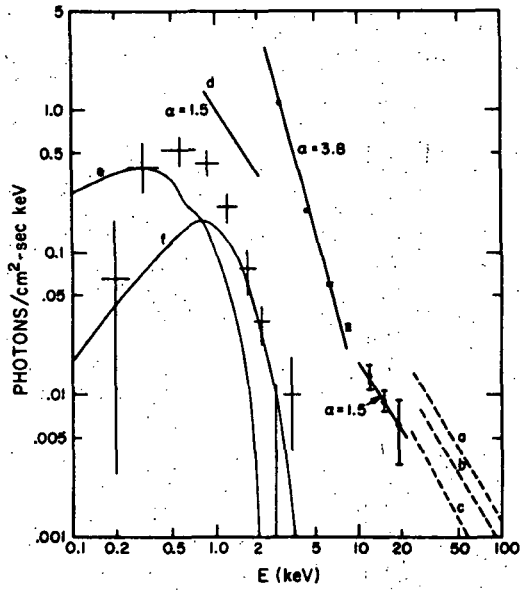

FIG. 1.—Spectrum of Cyg X-1 at various times. (Data points reported here are in counts per cm² per second per keV.) (*a*) $\alpha = 1.7$ Overbeck and Tananbaum 1968; (*b*) $\alpha = 1.9$ Haymes and Harnden 1970; (*c*) $\alpha = 2.1$ Webber and Reinert 1970; (*d*) representative spectrum reported here; (*e*) and (*f*) Cygnus Loop contribution and Cygnus X-1 spectrum plus 1.5×10^{21} H atoms cm^{-2} convolved with the detector response (counts cm^{-2} s^{-1} keV^{-1}), respectively. The solid-circle data points ($\alpha = 3.8$ and $\alpha = 1.5$) are from Schreier *et al.* (1971).

Cygnus Loop was determined with great accuracy, so that it is possible to reliably determine the contribution of the Loop to the data of Cyg X-1. The Loop spectrum plus the Cyg X-1 spectrum are combined for comparison with the observed data. Detailed measurements have been made of the collimator response and alignment with respect to the camera aspect reference. The contribution from the Loop does not introduce a large uncertainty in the total flux, but does degrade the determination of a spectral cutoff around 500 eV.

The very limited range of energies observed precludes the possibility of determining the spectral slope. Table 1 shows some representative parameters for an assumed spectral form of

$$J(E)dE = AE^{-\alpha} \exp(-\sigma_{BG} N_H) dE \text{ (photons cm}^{-2}\text{ s}^{-1}\text{ keV}^{-1}\text{)} .$$

TABLE 1

PARAMETERS FOR CYGNUS X-1

α	A	$N_H \times 10^{+21}$ H atoms cm^{-2}
1.5.....	1.11±0.14	1.5 ±0.32
2.5.....	1.8 ±0.16	3.99±0.37
3.5.....	2.76±0.23	6.04±0.37

The values of A and N_H corresponding to $\alpha = 1.5$ are favored from considerations of previous observations (Schreier *et al.* 1971; Gursky *et al.* 1971). It is clear that observations at energies above the upper limit of our detection system would be required to remove the ambiguity. The values for σ_{BG} were taken from Brown and Gould (1970).

We have examined the Cyg X-1 data for time variations during the scan. There is no clearly periodic structure evident as can be seen in figure 2, and the noise is essentially statistical, e.g., χ^2 of 69 for 99 degrees of freedom. There may be a flare just at the peak near 120 seconds; however, the statistical significance of the excess flux at this point is not easily determined. If the portions of the data excluding this region are fitted to a linear trial function (as would be expected for a uniform scan and a triangular collimator response function), then the two peaks near 120 s are about 9 σ above the expected value.

In order to verify that the detectors were operating normally, the spectrum of Cyg X-2, which was observed about 20 s later in the flight, has been reduced for comparison with previous observations. We find that the spectrum for Cyg X-2 is given by

$$J(E)dE = (1.4 \pm 0.4)E^{-1} \exp(-E/4.5) \exp(-\sigma_{BG}N_H)dE \text{ (photons cm}^{-2}\text{ s}^{-1}\text{ keV}^{-1}\text{)}$$

with

$$N_H = 0.8 \pm 0.4 \times 10^{21} \text{ H atoms cm}^{-2}.$$

E is measured in keV, and the temperature of 5.2×10^{7} ° K was taken from Bleach *et al.* (1972). This is quite consistent with the spectra obtained by Bleach *et al.* (1972) and Gursky *et al.* (1967) at higher energies, and the cutoff agrees with Hayakawa *et al.* (1971). The somewhat different intensity is within the observed variation of a factor of 1.6 reported by Giacconi *et al.* (1972). The absorption is reasonable for a distance of 500–900 pc as reported by Kraft and Demoulin (1967), Cathey and Hayes (1968), and Kristian, Sandage, and Westphal (1967), assuming a mean density of hydrogen of about 0.3 atoms cm^{-3}. The hydrogen columnar density through the Galaxy in this direction is about 1×10^{21} atoms cm^{-2} (H. Weaver, private communication).

After observing that the flux from Cyg X-1 was much below the level reported by Schreier *et al.* (1971), J. Kristian and C. Bolton were contacted to determine the phase of the B0 Ib star BD+34°3815 which has been identified as a possible optical candidate for the X-ray source. Both observers independently reported that the two stars were with 1–2 percent of a possible eclipse at this time, with the B0 Ib star in the near position and the unseen companion in the more distant position.

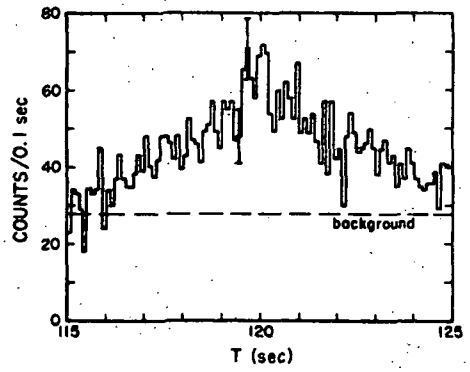

FIG. 2.—Observed transit of Cyg X-1. The energy range included is 0.5–3.0 keV. The possible large-amplitude pulsations occur at 119.5 and 120.0 s.

IV. DISCUSSION

In conclusion, Cyg X-1 has been observed during the period when it should be in eclipse, if in fact the X-ray source is associated with the companion of the star BD+34°3815 and the orbital inclination is such that eclipses occur. The observed flux is definitely in a low state; however, it is not lower than numerous observations made by *Uhuru* during 1971 December and 1972 January (E. Kellogg, private communication). The absorption in the spectrum is not statistically different in this state from that observed by Gursky *et al.* (1971). It is possible that the X-ray source responsible for the 1–10 keV radiation in the bright phase is not active at this time, thereby making an eclipse observation impossible. The flux observed during an inactive time may be from an envelope located around the B0 Ib star—perhaps similar to the Cen X-3 emission when the periodic source becomes quiescent, and during the eclipse phase of Cen X-3 (Schreier *et al.* 1972). Continued observations of Cyg X-1 are clearly required to establish the identity of the optical counterpart of the X-ray emitter.

Several points concerning this observation deserve comment. Both Cyg X-1 and Cyg X-2 show quite low absorption in their spectrum, and yet they are thought to be in a double or multiple star system from the optical data. Centaurus X-3 and 2U 1702+35 (Giacconi *et al.* 1972 and H. Tananbaum, private communication) are clearly part of a double or multiple star system based on their pulsed X-ray data, and show much higher X-ray cutoffs in their energy spectrum. The orbital periods of these two objects are substantially less than the periods for Cyg X-1 and Cyg X-2, if they have orbital periods at all, and suggest that the X-ray emitting objects may be moving in the tidally distorted atmosphere of their primaries. The lack of intrinsic absorption in the spectra of Cyg X-1 and Cyg X-2 may be taken to mean that they lie sufficiently far from their primaries that there is no interaction with the primaries' atmosphere.

Oda *et al.* (1971) have suggested that the X-rays from Cyg X-1 may originate from a region surrounding a collapsed object. If the identification with BD+34°3815 is correct, the unseen companion may have sufficient mass to add weight to this speculation (cf. Webster and Murdin 1972). On the other hand, it is difficult to understand how matter accreting onto such an object could produce quasi-periodic intensity fluctuations of large amplitude.

Jackson (1972) has proposed a model to explain the hard X-ray observations in terms of inverse Compton scattering between electrons produced in a pulsar and photons produced by the B0 Ib star. This model predicts time variations on the order of 3000 s. If the results reported in this communication are taken to be an extrapolation of the balloon data, and hence produced in the same way, then the timescale for the suggested variations shown in figure 2 is much too short for the Compton-scattering origin. Perhaps, as Jackson has suggested, the pulsating portion is generated by an independent mechanism and appears very weak at the time of these observations.

The authors wish to thank the staffs of the Sounding Rocket Branch of the Goddard Space Flight Center and the White Sands Missile Range for their support of the Aerobee launch. We acknowledge useful conversations with H. Tananbaum at American Science and Engineering concerning the pulsating source in Hercules; and J. Kristian of the Hale Observatories and C. Bolton of David Dunlap Observatory concerning the phase of the companion of BD+34°3815. We thank Dr. H. Weaver at the University of California at Berkeley for providing the value of the H I in the direction of Cyg X-2 prior to publication. We also thank B. Baaquie, P. Gloger, C. Sarazin, S. Speer, and F. Yates of California Institute of Technology for supporting the effort. This work was supported in part by National Aeronautics and Space Administration grants NGL 05-002-007 and ~~NGL 05-002-207.~~

NGR 05-002-219

REFERENCES

Bleach, R. D., Boldt, E. A., Holt, S. S., Schwartz, D. A., and Serlemitsos, P. J. 1972, *Ap. J.*, **171**, 51.
Brown, R. L., and Gould, R. J. 1970, *Phys. Rev. D*, **1**, 2252.
Cathey, Larry, R., and Hayes, James E. 1968, *Ap. J.* (*Letters*), **151**, L89.
Garmire, G., and Riegler, G. 1972 (to be published).
Giacconi, R., Gursky, H., Kellogg, E., Murray, S., Schreier, E., and Tananbaum, H. 1972 (to be published).
Gursky, H., Gorenstein, P., and Giacconi, R. 1967, *Ap. J.* (*Letters*), **160**, L85.
Gursky, H., Gorenstein, P., Kerr, F. J., and Grayzeck, E. J. 1971, *Ap. J.* (*Letters*), **167**, L15.
Hayakawa, S., Kato, T., Kohno, T., Nishimura, K., Tanaka, Y., and Yamashita, K. 1971, *Nature Phys. Sci.*, **231**, 76.
Haymes, R., and Harnden, F. 1970, *Ap. J.*, **159**, 1111.
Jackson, J. C. 1972, *Nature*, **236**, 39.
Kraft, R., and Demoulin, M.-H. 1967, *Ap. J.* (*Letters*), **150**, L99.
Kristian, J., Sandage, Allan, and Westphal, J. A. 1967, *Ap. J.* (*Letters*), **150**, L99.
Oda, M., Gorenstein, P., Gursky, H., Kellogg, E., Schreier, E., Tananbaum, H., and Giacconi, R. 1971, *Ap. J.* (*Letters*), **166**, L1.
Overbeck, J., and Tananbaum, H. 1968, *Phys. Rev. Letters* **20**, 2A.
Schreier, E., Gursky, H., Kellogg, E., Tananbaum, H., and Giacconi, R. 1971, *Ap. J.* (*Letters*), **170**, L21.
Schreier, E., Levinson, R., Gursky, H., Kellogg, E., Tananbaum, H., and Giacconi, R. 1972, *Ap. J.* (*Letters*), **172**, L79.
Webber, W. R., and Reinert, C. P. 1970, *Ap. J.*, **168**, 883.
Webster, B. L., and Murdin, P. 1972, *Nature*, **235**, 37.

X-RAY SPECTRUM OF THE ENTIRE CYGNUS LOOP

J. C. Stevens*, G. R. Riegler†, and G. P. Garmire

California Institute of Technology

Pasadena, California

Received 1973 January 3

*Present address: Lawrence Livermore Laboratory, Livermore California

†Present address: Bendix Corporation, 3300 Plymouth Rd., Ann Arbor, Michigan 48105

ABSTRACT

The spectrum of the entire Cygnus Loop has been obtained using gas filled proportional counters and filters flown on a Nike-Aerobee rocket. The results indicate an average spectral temperature of $(2.8 \pm 0.2) \times 10^6$ °K and the presence of excess emission in the energy range (0.530 - 0.693) keV. If the excess emission originates in a single line at 0.658 keV the intensity at the earth corresponds to $1.8 \pm .7$ photons/cm^2-sec or about ten percent of the total energy received from the Loop. The spectrum of the entire Loop is found to be attenuated by an average of $(4.8 \pm 0.2) \times 10^{20}$ hydrogen atoms/cm^2.

Subject Headings: Nebulae - Spectra, X-Ray - Supernovae Remnants - X-Ray Sources

I. INTRODUCTION

The observed expansion of the filaments of the Cygnus Loop (Minkowski 1958) led Shklovsky (1968) to predict that this object should be a thermal bremsstrahlung source of x-rays with a temperature of 2.5 million degrees. The first x-ray observations to clearly identify the Loop as a source were made by Grader et al. (1970). They found that the Loop emitted x-rays primarily in the 0.2 - 1.5 keV band, but did not have sufficient data to distinguish between a thermal (exponential) or non-thermal (power law) spectral form. In 1970 Gorenstein and co-workers examined the Cygnus Loop in the soft x-ray range of energies using a one-dimensional focusing telescope system (Gorenstein et al. 1971). They succeeded in obtaining a one-dimensional "strip" scan of the object showing that the emission was confined to the region of the optical emission along one axis. In addition, they obtained a spectrum of the entire Loop which was best characterized as thermal bremsstrahlung with line emission at about 650 eV. They determined the x-ray spectral temperature to be 4.2 million degrees. The term "spectral temperature" is taken to mean the empirical e-folding parameter used to fit the data and should not be taken to imply a plasma temperature directly.

Line emission at approximately 650 eV is expected from a plasma containing collisionally-excited multiply-ionized oxygen atoms as suggested

by the above authors. These atoms radiate strongly at temperatures between 2 and 4 million degrees (Shklovsky 1968, and Tucker and Koren 1971), and give rise to several lines clustered around 575 and 650 eV. The presence or absence of these lines furnishes us with a test of the nature of the x-ray emission mechanism. The presence of line emission is a clear indication of thermal emission, even if large temperature and density variations are present as suggested by the complex surface brightness distribution (Stevens and Garmire 1973). In the radio band of the spectrum non-thermal processes are clearly indicated by the polarization observations of Kundu (1969), Moffat (1971), and Kundu and Becker (1972). Whether the synchrotron process can provide a portion of the x-rays in the Cygnus Loop cannot be ruled out completely by the observation of line emission; however, the importance of this process can be limited by studies of the line to continuum strengths should such lines be detected.

II. EXPERIMENT DESCRIPTION

The Cygnus Loop was observed on 23 October 1971 at 03:47 UT for 140 seconds by detectors on board an Aerobee 170 rocket launched from White Sands Missile Range. The basic detectors employed were four multi-anode proportional counters which are described by Garmire and Riegler(1972). The detector was constructed in three equal layers separated by ground plane wire grids. Results are only presented for the layer adjacent to the window (W) and the middle layer (M). The third layer against the back wall of the detector had a low signal to noise ratio and was not used. Two of the detectors were fitted with mechanical collimators which provided a narrow fan beam for mapping purposes, the results of which were reported

by Stevens and Garmire (1973). The remaining two detectors were fitted with broad field of view mechanical collimators to provide spectral data during the entire period that mapping was being performed by the other two detectors. A large field view was permitted since the Cygnus Loop is well isolated from other sources of soft x-ray radiation. The basic detector characteristics are shown in Table 1. The energy response of the detectors included two nominal energy bands (0.2 - 0.28) keV and (0.4 - 2.5) keV. The filters serve to substantially modify these basic responses, and are shown in figures 3 and 4, together with the unfiltered response. The figure captions give the notation referred to in the tables in the text.

Proportional counters have quite poor energy resolution at the energy of the anticipated oxygen emission (approximately 60% at 650 eV). For this reason one detector (D) was fitted with a gas cell and a solid filter flap of teflon which could be rotated in front of the detector. By admitting pure oxygen gas into the gas cell, a narrow region of transmission could be obtained just below 0.532 keV (above 23.3 $\mathring{A}$), which is below the

anticipated ionized oxygen emission and could be used to determine the continuum strength at that point (see figures 3 and 4). The teflon filter transmitted a narrow band just below 0.693 keV (above 17.9 Å) which should include the O VII and several of the O VIII lines (see figures 3 and 4). The other detector (C) was used to obtain an energy spectrum based purely on the energy resolution of the proportional counter.

An $Al_{K\alpha}$ x-ray line produced by Po^{210} α-ray excitation of an aluminum foil was attached to the door of the experiment compartment of the rocket, thereby providing an energy calibration at the beginning and end of the flight. The detectors exhibited less than a 5% gain variation during the flight. The linearity of the detector system was measured at six energies between 0.28 and 2.8 keV in the laboratory. No deviation from linearity greater than 2% in this energy range was observed.

III. OBSERVATIONS

The scan path of the detector system over the Cygnus Loop was reported by Stevens and Garmire (1973). The counting rate versus time for counters C and D are shown in figure 1. The time from 140 to 275 seconds after launch was spent scanning the Loop. The filtered measurements were performed between 145 to 215 seconds. Detector C was unfiltered throughout the measurement as was detector D between 250 to 275 seconds. (The 250 second point was chosen as the time when oxygen gas was completely exhausted from the gas cell.)

Oxygen gas was admitted to the gas cell between 144 and 173 seconds. The teflon filtered observations of the Loop were made from 202 to 212 seconds. The x-ray fluxes during these times were obtained by subtracting the instrumental background counting rate from the rate with the filter in position.

The instrumental rates were obtained at 82 to 94 and 363 to 367 seconds into the flight when the detectors were deep in the earth's atmosphere and the teflon filter was over detector D. The average counting rates observed during these times for detector D are given in Table 2. To obtain the true fluxes the observed counting rates must be corrected for the changes in the pointing direction of the rocket. The average correction factor was found to be 2.5 for the oxygen filter and 1.7 for the teflon. The resultant fluxes after instrumental background has been subtracted are given in the last column of Table 2.

In addition to the corrections for changes in the orientation of the rocket during the observation, two other corrections were necessary. During the oxygen filter measurement the altitude of the rocket ranged from 152 km to 169 km. Attenuation by atmospheric nitrogen and oxygen introduces a correction at 0.4 keV of between 8 and 4 percent. This is small compared to statistical uncertainties. The teflon filter measurements were made above 175 km where the atmospheric correction is negligible. However, the oxygen gas in the gas cell was not completely exhausted during the teflon measurements and ranged from about 74 to 45 $\mu gm/cm^2$ in thickness. The residual oxygen attenuated the potential line at 658 eV by between 70 and 50%. During the oxygen filter measurements the thickness of oxygen gas corresponded to 390 ± 10 $\mu gm/cm^2$. The thickness of oxygen gas was measured by measuring the pressure in the gas cell using a potentiometric transducer, and the temperature was monitored to within $\pm 2^{\circ}C$ by thermistors attached to the gas cell.

IV. DATA ANALYSIS

The analysis of the filtered and the unfiltered data was made by folding trial input spectra attenuated by interstellar gas with the measured detector response and resolution parameters (see Gorenstein et al. 1968). A total of 7000 counts were used in the filtered measurements and 50,000 counts in the unfiltered observation.

The trial input continuum spectra used to obtain a fit to the data were of the form

$$dN/dE = AE^{-\alpha} \exp(-\sigma_{BG}(E)N_H) \text{ photons/cm}^2 \text{ sec keV} \quad (1)$$

and

$$dN/dE = BE^{-1} \exp(-E/kT - \sigma_{BG}(E)N_H) \text{ photons/cm}^2 \text{ sec keV}, \quad (2)$$

where $\sigma_{BG}(E)$ represents the absorption cross-section of the interstellar gas computed by Brown and Gould (1970) and N_H is the columnar density of hydrogen in atoms/cm^2. These input spectra were not chosen on the basis of any compelling physical arguments; however, many other x-ray sources have been found to follow spectral shapes of this form. Line emission was added to both trial spectra in the form of $I(E_o)\delta(E-E_o) \exp(-\sigma_{BG}(E_o)N_H)$, where $I(E_o)$ and N_H are free parameters and E_o was chosen to be either 0.575 or 0.658 keV corresponding to the regions of the O VII and O VIII emission. The free parameters were varied until acceptable χ^2 fits were obtained with the data for the various detectors. A superposition of exponential spectra at a number of temperatures can simulate a power law spectrum over a limited range of energy (Klimas and Sandri 1969) so that adding spectral lines to a power law spectrum is not unfounded.

At first it might appear that the filtered data only need be compared in the energy range of the pass bands of the filters. After attempting this analysis, it was found that the results were quite sensitive to the choice of bandwidths accepted for the transmission regions. The reason for this sensitivity lies in the steep fall off of the Loop spectrum near 1 keV and the very poor detector resolution near 0.6 keV (about 0.4 keV). For this reason, the entire filtered spectrum was fitted by the trial input spectra rather than a narrow region. No diffuse x-ray background was subtracted from the filtered data. There are several reasons for not subtracting an x-ray background. First, the diffuse flux entering the detector field of view is only about 10% of the Cygnus Loop flux at 0.6 keV. Second, the actual diffuse spectrum in the region of the Cygnus Loop is not measured well at 0.6 keV, thereby making a background subtraction rather arbitrary. Finally, the deduced strength of the excess emission in the teflon filter is based on the relative strength between the teflon and oxygen filtered fluxes, and for this reason is only weakly dependent upon the subtraction of a flux value from both intensities for small backgrounds. In the case of the unfiltered measurements, the diffuse flux obtained at 290 seconds was subtracted from the Cygnus Loop plus background data. The subtraction is necessary in the case of the unfiltered data, since the shape of the background spectrum is quite different from the shape of the Cygnus Loop spectrum. The low and high energy regions of the Loop spectrum are most strongly affected by the subtraction, since the background spectrum is much flatter than the spectrum of the Loop. The subtraction represents a possible source of systematic error.

V. SPECTRAL RESULTS

The results of the unfiltered analysis were obtained in a manner identical to numerous spectra found in recent literature (see Gorenstein et al. 1968).

The middle layer of detectors C and D, consisting of four cells, was subdivided into a set of detector cells adjacent to the walls of the counter and the middle two cells away from the counter walls. This combination permitted six independent measurements of the spectral parameters of the Cygnus Loop. Four trial input spectra were fitted to the data; namely, an exponential spectrum, a power law spectrum, an exponential spectrum with two lines at 0.575 and 0.658 keV, and a power law spectrum with two similar lines. Acceptable fits to the data were obtained for an exponential plus line emission and a power law plus line emission as shown in Table 4.

The six independent unfiltered measurements were found to provide spectral parameters which varied by somewhat more than expected on a purely statistical basis. Considerable calibration effort was made to reduce the measurement errors, but the remaining systematic errors evidently dominate the precision of the final result. The quality of the best fit to CW data is shown in figure 2. The systematic accuracy of any given measurement is not a priori any better than any other; therefore, the results have been weighted by their statistical errors and combined to find a mean value and are given below. Another possible explanation for the discrepancy is that the trial input spectra are not correct and that an improved spectrum would provide a better fit to the data. Indeed, if a plasma emission spectrum with cosmic abundance of elements is correct, many other emission lines are present, as have been observed in the solar spectrum, for example see Walker (1972). This point is discussed in the next section.

The teflon filtered data provide a measure of the excess emission that occurs in the (0.53 - 0.69) keV band. The oxygen filter provides a measure of the continuum and line emission in the (0.44 - 0.53)keV band. The first

indication of the fact that there is excess emission in the teflon filter band is shown in Table 3. The continuum level parameters B (eq. (2)), which fit the teflon filter data for the trial spectra given in Table 4 are significantly higher than the equivalent parameters for the oxygen data, thus indicating excess emission in the (0.53 - 0.69) keV band.

Making the assumption that all of the energy in the (0.53 - 0.69) keV comes from a single line at 0.658 keV plus the continuum radiation in this band, the best value for this line intensity is 2.3 ± 0.9 photons/cm^2 sec. The best mean spectral parameters using the filtered and unfiltered data combined are then

$$dN/dE = [((150\pm30)/E)\ \exp\ (-E/_{(.25\pm.02)})]\ \exp\ [-\sigma_{BG}(4.8\pm.2)\ x\ 10^{20}]\text{ph/cm}^2\text{-sec-keV}$$

$$+\ (2.3\pm.9)\ \delta(E-0.658)\ \exp\ (-\sigma_{BG}\ (4.8\pm.2)\ x\ 10^{20})\ \text{ph/cm}^2\text{-sec.} \qquad (3)$$

The unfiltered data provided the parameters for the continuum and the absorption, whereas the line strength was taken from a combination of the filtered and unfiltered data.

VI. DISCUSSION

The best fit to the above data shows that about 10% of the emission received at Earth from the Cygnus Loop could originate in a line at around 0.658 keV. This is obviously a great oversimplification, but it provides a basis for comparison with model calculations.

An alternative way to represent the data is to assume a model plasma with a uniform temperature (almost certainly a poor assumption) and compute the total energy received in the oxygen lines near 0.575 and 0.658 keV. At 2.8×10^6 °K we compute a ratio for I (.575)/I(.658) of 3.3. The detector plus filter efficiencies shown in Figures 3 and 4 reveal that there is a substantial decrease in efficiency for detection of the 0.575 keV region. The lower efficiency implies that a more intense flux of 0.575 keV radiation is required to produce the same excess counting rate. To an adequate approximation the flux required to fit the filtered data can be satisfied by a linear combination between I (.575) and I (.658) of the form I (.575) x ρ + I (.658) x (1-ρ) where $0 \geq \rho \geq 1$, and I (.575) = 7.0 ± 2.8 ph/cm^2 sec. Taking the ratio of 3.3 to be the expected value for these lines at 2.8×10^6 °K, the intensities of the lines near 0.575 keV and 0.658 keV are 3.3 ± 1.2 and 1.0 ± 0.4 respectively. This is about 25% of the energy received from the Loop at the Earth.

The unfiltered data tend to limit the amount of energy that can go into the spectral region around 0.575 keV. The best values from the six unfiltered measurements for the contribution at 0.575 keV are quite discrepant. The largest value allowed is about 4.1 photons/cm^2-sec, which is 2.7 ph/cm^2-sec at the Earth. It is interesting to note that an optically thin plasma possessing an elemental abundance similar to the sun in equilibrium at 2.8×10^6 °K would radiate nearly 50% of its energy in the oxygen lines. This number includes the absorption of photons by the interstellar medium observed for the Cygnus Loop.

These results should be taken only as indicative, in that the temperature obtained by using a more complex spectrum to fit the data will be different from that obtained by a simple exponential plus a single line. A single temperature is an additional weak assumption, in that large spatial inhomogeneities are revealed in the map of Stevens and Garmire (1973), which are likely to be associated with temperature variations. In addition to the uncertainties in the temperature of the plasma, the assumption of local thermodynamic equilibrium used to compute the line intensities may not be correct. That this may be the case can be seen from the recombination time of OV III, for a gas density in the Loop of a few ions/cm^3. The recombination times will be of the order of 10^4 years or of the order of the age of the Loop.

ACKNOWLEDGEMENTS

The authors wish to thank B. Baaqui, F. Cordova, W. Moore, C. Sarazin, S. Speer and F. Yates of the California Institute of Technology for supporting this effort. The Sounding Rockets Branch of the Goddard Space Flight Center and the White Sands Missile Range have generously contributed their support to this flight. This work was funded for the major portion by the National Aeronautics and Space Administration grant NGR 05-002-219.

TABLE 1

NOMINAL DETECTOR CHARACTERISTICS

Detector	Window Thickness (Polypropylene-μg cm^{-2})	Geometric Area	FOV (FWHM)	Energy Band (keV)
C	140 (μgm/cm^2)	395 (cm^2)	12^o x 12.3^o	0.2-2.5
D	271 (μgm/cm^2)	425 (cm^2)	9.3^o x 10.0^o	0.2-2.5

TABLE 2

DETECTOR D COUNTING RATES AND FLUXES (0.25 to 2.5 keV)

Detector	Filter	Time Interval (sec)	Average Counting Rate (counts/sec)	Net Corrected Flux (counts/sec)
Window				
	No filter	82.0 to 93.9 plus 363.0-366.9	39.6 ± 1.5	
	O_2 filter	144.0 to 172.9	62.6 ± 1.5	58.1 ± 5.3
	Teflon	202.0 to 211.9	54.9 ± 2.3	25.9 ± 4.7
Middle		82.0 to 93.9 plus 363.0 to 366.9	8.5 ± 0.7	
	O_2 filter	144.0 to 172.9	15.0 ± 0.7	16.4 ± 2.5
	Teflon	202.0 to 211.9	12.2 ± 1.1	6.3 ± 2.2

TABLE 3

CONTINUUM LEVELS CONSISTENT WITH FILTERED MEASUREMENTS

Detector Layer	Filter Material	Continuum level (B) for trial spectral parameters			
	kT (keV)	0.23	0.24	0.26	0.28
	$N_H \times 10^{-20}/cm^2$	5.8	5.2	4.5	3.9
Window	Oxygen	185 ± 17	157 ± 14	119 ± 11	93 ± 8.5
Middle	Oxygen	184 ± 28	147 ± 22	105 ± 16	77 ± 12
Window	Teflon	350 ± 60	290 ± 50	210 ± 40	165 ± 30
Middle	Teflon	270 ± 90	210 ± 80	150 ± 50	106 ± 37

TABLE 4

SUMMARY OF SPECTRAL PARAMETERS OBTAINED FROM UNFILTERED DETECTORS

Model*	Continuum	kT (keV)	α	$N_H \times 10^{-20}$	I_o (0.658) Ph/cm^2 sec
Exp + L	130 ± 30	0.25 ± .02	....	4.8 ± 0.2	1.4 ± 0.5
PL + L	2.1 ± 1.1		4.4 ± 0.3	5.5 ± 0.4	2.3 ± 0.5

* EXP and PL are for exponential and power law trial input spectra as given in equations (1) and (2). The "L" stands for line emission in the form of a delta function input. The spectral fits obtained without line emission possessed unacceptably large χ^2 values. The errors were obtained by varying each parameter until the χ^2 increased by one unit.

REFERENCES

Brown, R. and Gould, R. 1970, Phys. Rev. D, 1, 2252.

Garmire, G. P., and Riegler, G. R. 1972, Astron. and Astrophys., 21, 131.

Gorenstein, P., Gursky, H., and Garmire, G. 1968, Ap. J., 153, 885.

_____, Harris, B., Gursky, H., Giacconi, R., Novick, R., and Van den Bout, P. 1971, Science, 172, 369.

Grader, R.J., Hill, R.W., and Stoering, J.P. 1970, Ap. J. Lett., 161, L45.

Klimas, A., and Sandri, G. 1969, ARAP Tech. Memo 69-8.

Kundu, M. R. 1969, Ap. J., 158, 103.

_____, and Becker, R. H. 1972, Astron. J., 77,459.

Minkowski, R. 1958, Rev. Mod. Phys, 30, 1048.

Moffat, P. H. 1971, MNRAS, 153, 401-412.

Shklovsky, I. S. 1968, Supernovae, (New York: Interscience Pub.)

Stevens, J. C., and Garmire, G. P. 1973, Ap. J. Lett. Feb. 15.

Tucker, W. H., and Koren, M. 1971, Ap. J., 168, 283.

Walker, A. B. C., Jr. 1972, Space Sci. Rev., 13, p672.

FIGURE CAPTIONS

Fig. 1 - Counting rate versus time in the 0.2 - 2.5 keV band for the detector C and D window layers.

Fig. 2 - The best fit spectrum to the detector C window layer. The spectral parameters are for a exponential spectrum. (eq. 2) at a temperature of 0.24 keV attenuated by 4.9×10^{20} H atoms/cm^2. A line at 0.658 keV of 0.5 ph/cm^2 sec has been included to obtain the best fit to this data.

Fig. 3 - The detection efficiency versus energy for the window layers of the C and D detectors. The "O" refers to the oxygen filter transmission in the DW detector and the "F" refers to the teflon (flourine edge) filter in the DW detector.

Fig. 4 - The detection efficiency versus energy for the middle layers of the C and D detectors. The "O" refers to the oxygen filter transmission in the DM detector and the "F" refers to the teflon (flourine edge) filter in the DM detector.

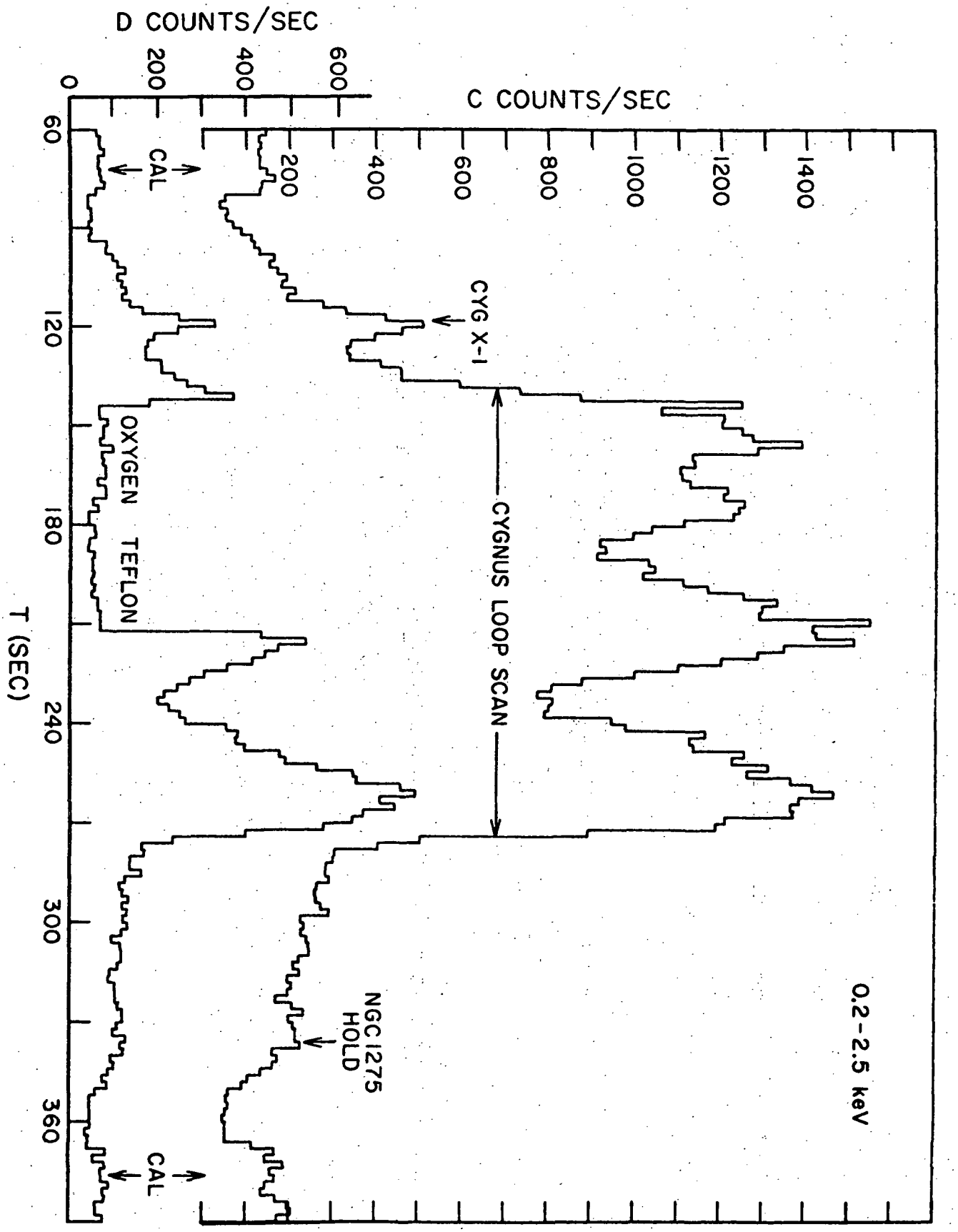
D COUNTS/SEC
0
200
400
600
C COUNTS/SEC
200
400
600
800
1000
1200
1400
T (SEC)
60
120
180
240
300
360
CAL
CYG X-1
OXYGEN TEFLON
CYGNUS LOOP SCAN
NGC 1275 HOLD
CAL
0.2-2.5 keV

Figure 1

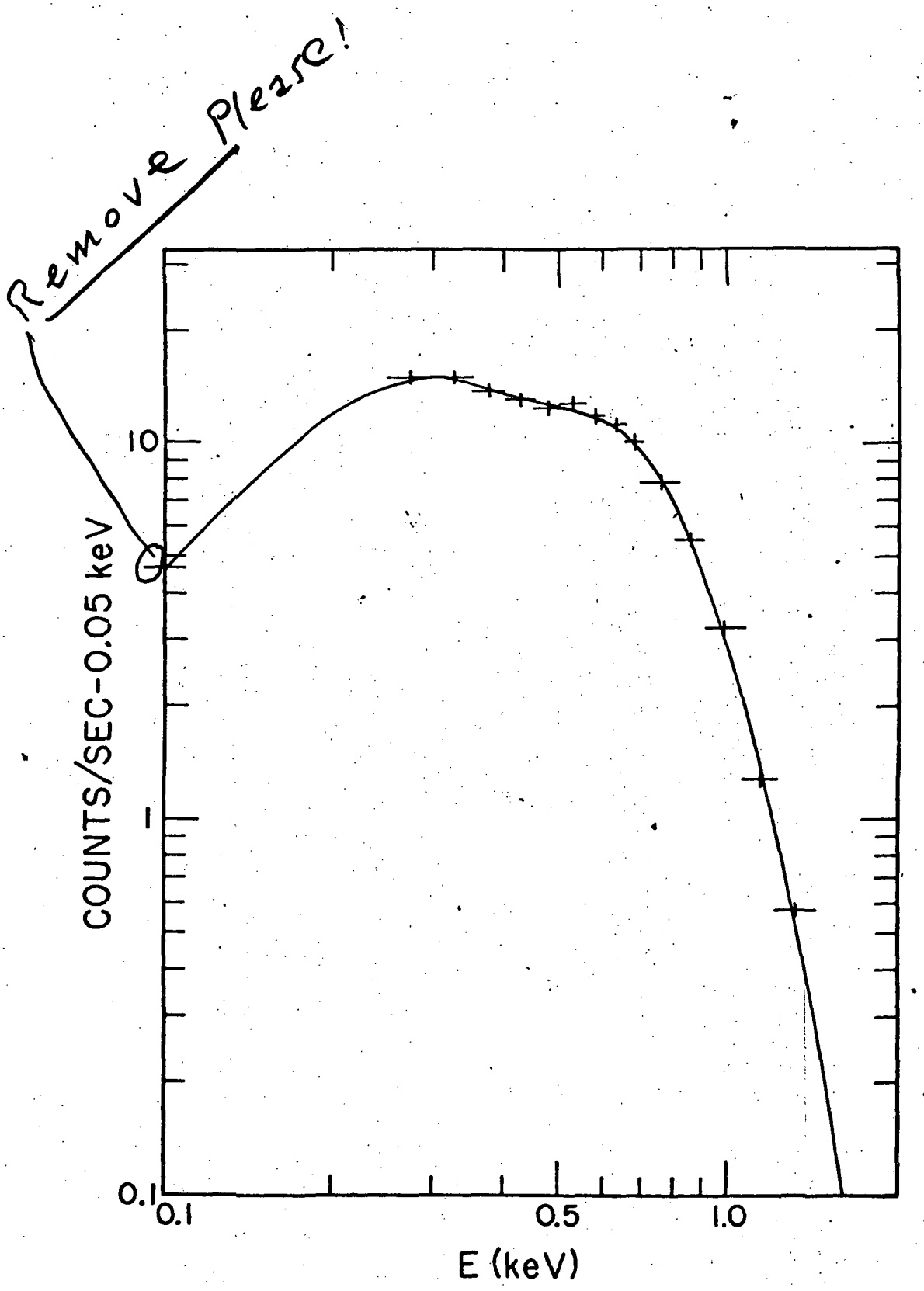

Figure 2

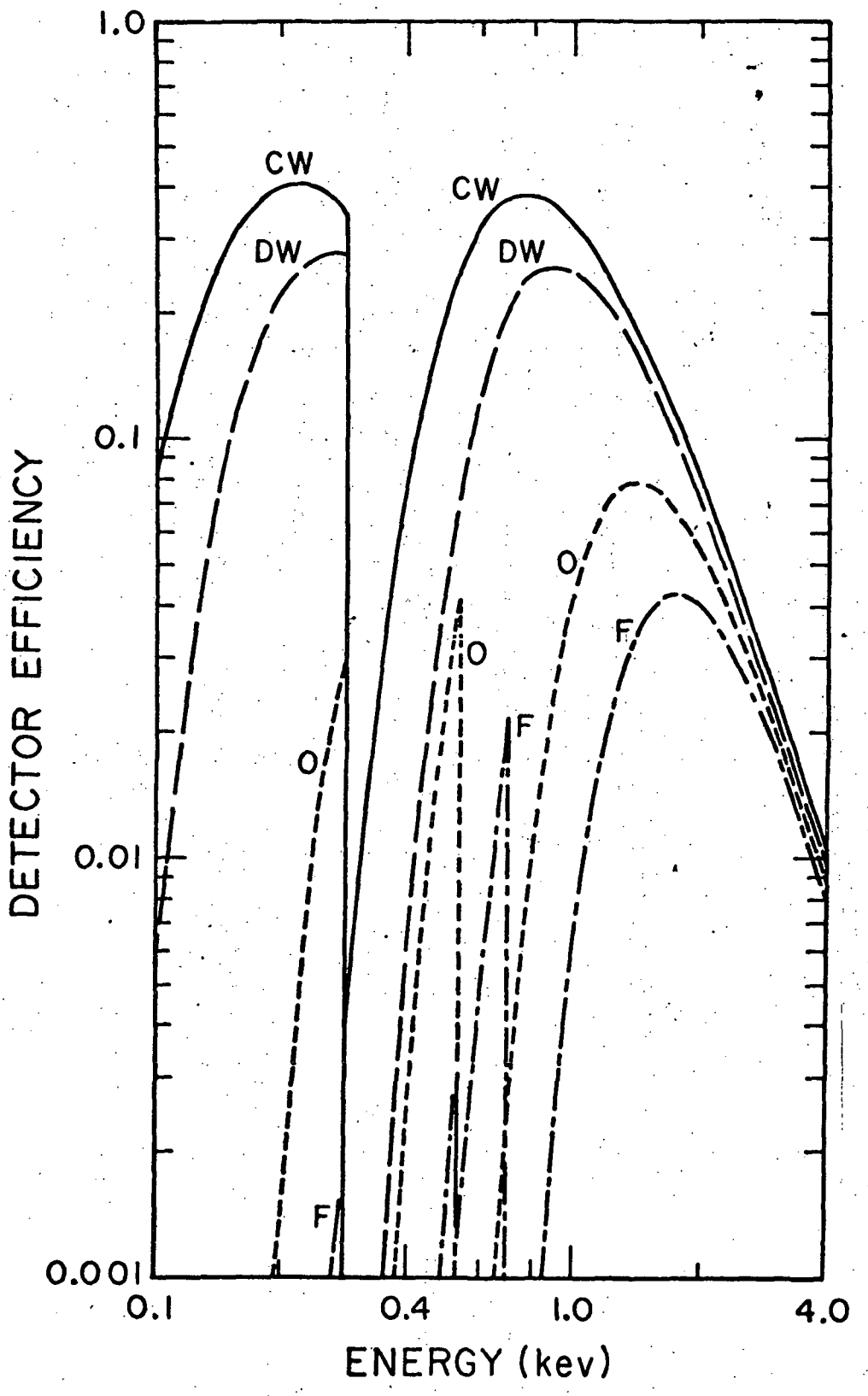
1.0
0.1
0.01
0.001
DETECTOR EFFICIENCY
CW
DW
O
F
CW
DW
O
F
O
F
0.1
0.4
1.0
4.0
ENERGY (kev)

Figure 3

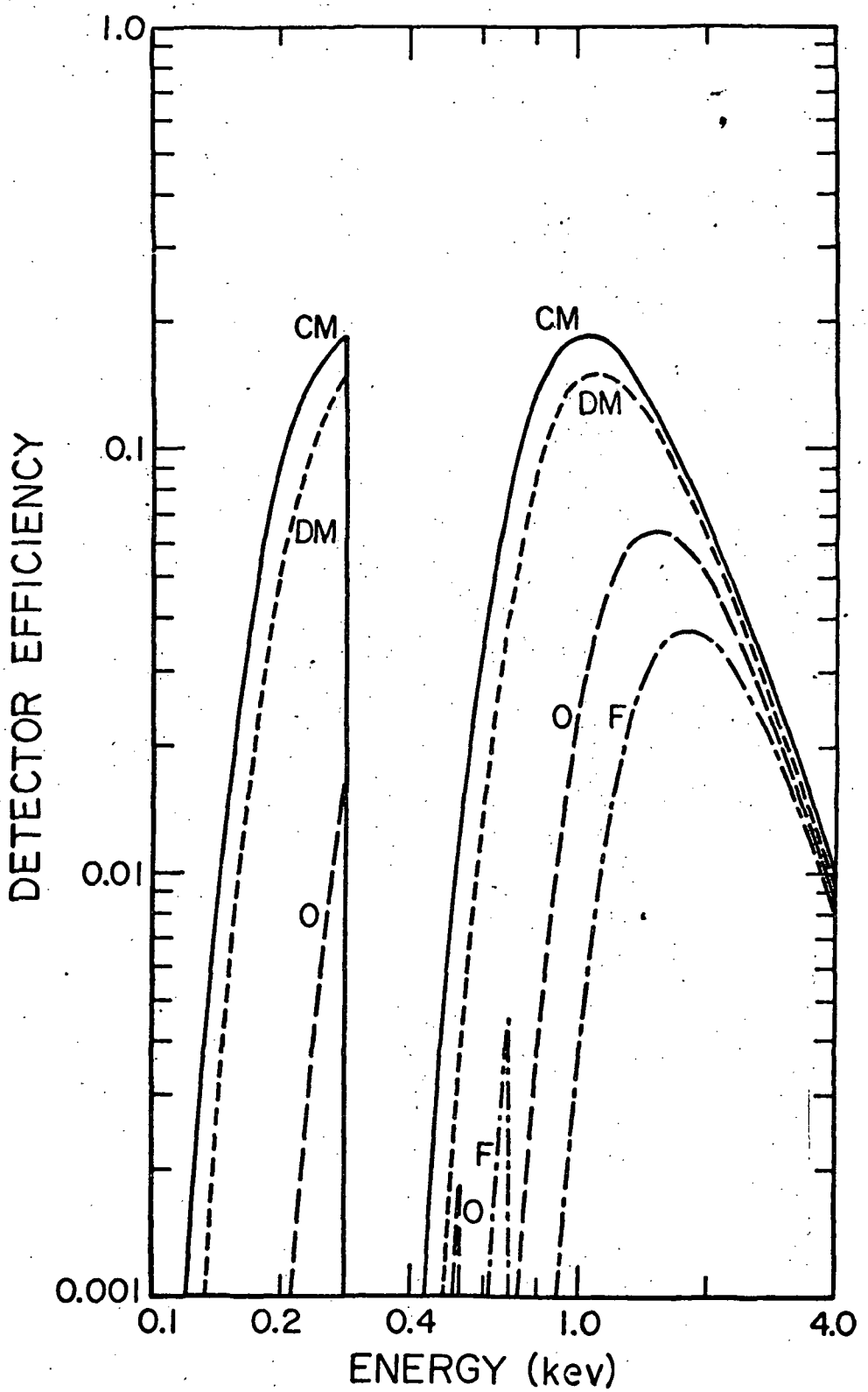
1.0
0.1
0.01
0.001
DETECTOR EFFICIENCY
CM
DM
O
CM
DM
O
F
F
O
0.1
0.2
0.4
1.0
4.0
ENERGY (kev)

Figure 4

THE X-RAY SURFACE BRIGHTNESS OF THE CYGNUS LOOP

J. C. Stevens* and G. P. Garmire

California Institute of Technology

Pasadena, California

Received October 26, 1972

*Present address: Lawrence Livermore Laboratory, Livermore California

ABSTRACT

The surface brightness of the Cygnus Loop in x-rays was obtained on a scale of 0.25 deg^2. The x-ray emission shows strong limb-brightening implying a shell-like source structure. The shell exhibits several regions of enhanced emission. X-ray emission which was observed from a region near the center of the Loop may be from a remnant object. The correlation between the x-ray and optical emission is not as good as the correlation between radio and optical emission.

I. INTRODUCTION

A soft x-ray experiment aboard an Aerobee 170 rocket was launched from White Sands Missile Range on 23 October 1971 at 03:45:00.5 U.T. During the middle of the flight, from 140 s to 270 s after launch corresponding to an altitude greater than 153 km, the Cygnus Loop was observed using four proportional counter detectors fitted with mechanical collimators. The detectors were identical to those described by Garmire and Riegler (1972). Only two of the four detectors were used for the x-ray mapping of the Cygnus Loop. Their parameters are discussed in the Appendix. The other two detectors were used for spectral studies. The spectral results will be presented in another place.

X-ray emission from the Cygnus Loop has been seen by Grader et al. (1970), Gorenstein et al. (1971), and probably reported by Henry et al. (1968) who detected a source Vul XR-1 in the same general region of the sky. One of the objectives of the observations made during this rocket flight was to provide a detailed x-ray map of the Cygnus Loop for comparison with optical and radio data. This aspect is reported below.

II. OBSERVATIONS

The Cygnus Loop was scanned four times by each detector during the 130-second observing period. The scan path and observed counting rates are shown in figure 1. The data include the nominal energy band 0.2 - 1.5 keV. The direction of each point along the scan was determined to about ±5 arc minutes through star field photographs taken once per second. There were at least three stars observable in the camera's 8^{o} x 12^{o} field of view at all times during the scan.

The angular extent of the x-ray emission can be obtained by noting the times when the detector count rates rise substantially above background, then constructing the lines of the collimator transmission peak at these times.

Several representative acquisitions are indicated by the numbers in figure 1. Lines corresponding to the detector transmission directions are drawn to indicate the boundaries of the x-ray emitting region. The difference in intensity observed between the A and B detectors during the transit of the Loop from 256-267 sec, is the result of a pre-flight drift in the gas pressure control system which produced effectively different threshold discriminator settings, A being about 250 eV and B about 150 eV.

A much more detailed analysis is required to obtain the best intensity distribution consistent with all aspects of the data. The method employed is described fully in the Appendix, and only a brief description follows. The sky in the region scanned was divided arbitrarily into 4761 cells, each 0.5^{o} x 0.5^{o} on a side, positioned in a 69 x 69 cell square array centered near the Cygnus Loop. This array completely encompassed the region scanned by the edges of the collimator fields of view. For each second of time, counts are added to the cells sampled by the collimator to make up the observed intensity after the mean background has been subtracted. These counts are weighted by the collimator response. This addition of counts was done in a sequential fashion, the modified source distribution from one time interval being used as the trial source distribution for the next time interval. Since the Cygnus Loop region was scanned eight times this sequential modification process resulted in cancellation in the low intensity regions and reinforcement in regions of high intensity. This process was iterated until a pattern emerged that appeared stable.

The entire set of data between 140 and 270 seconds was inverted by the iterative process. The only regions obtained above background were the Cygnus Loop and a strip corresponding to the single transit of Cyg X-1 through the field of view of detector A at 197 seconds. A total of 30 iterations were required before a stable pattern emerged. After only ten iterations through the 260 data points (two collimators with 130 data points, each comprised

of one-second integrations) a pattern very similar to the final distribution was obtained, except for faint "wings" to the northeast and to the northwest of the Loop. The region of these "wings" was the area most poorly sampled by the scans. The "wings" were set to zero on the basis of the direct limitation on the extent of the emission obtained by examining figure 1. After ten more iterations the "wings" were detectable, but at a much reduced level. This process was then repeated a third time, and the "wings" completely disappeared into the noise.

The final map shown in figure 2 was obtained directly from the iterative process. A second process derived the structure using intuition plus trial and error. This process was carried out simultaneously and independently with the computer analysis. The resulting rough map showed the same essential configuration. Changes in the trial element size produced only slight changes in the spatial structure consistent with the changes in the trial function (S_{ij} in the Appendix). A single bar in figure 2 represents 0.8% of the total intensity of the Loop or about 10^{-10} ergs/cm^2/s/0.25 deg^2 observed at the earth in the 0.2 - 1.5 keV band. Horizontal bars are negative differences and the one-sigma noise on each cell is about ±2 bars. The noise was determined by the observed fluctuations in the background cells outside the Loop, not from the number of counts in each S_{ij} element. The noise was about twice that expected from fluctuations on the number of counts. The total intensity at the earth obtained in the above energy range is (1.3 ± 0.2) x 10^{-8} ergs/cm^2-sec. The spectrum of the entire Loop yields a temperature of 2.8 x 10^6 ^{o}K. More detailed spectral results will be reported elsewhere.

The resulting emission regions were examined for gross spectral variations by dividing the observed counting rate data into two energy bands containing roughly equal numbers of counts, namely 0.2 - 0.56 and 0.56 - 1.5 keV. The actual incoming x-ray energies sampled in these divisions are 0.2 - 0.28 and 0.45 - 1.5 keV, but resolution spreading in the detector fills in the region

between 0.28 and 0.45 keV, where the detector window transmission is very small. No statistically significant differences were observed between the brightest regions. The results are shown in Table 1, where the numbers in parentheses are the fraction of the intensity above 0.56 keV. No fraction is given for intensities below 2.9% since the errors are very large for these values.

III. DISCUSSION

The x-ray structure of the Cygnus Loop has been determined to a scale of 0.5^{o}. The strong limb-brightening shows that the x-rays are produced primarily in the outer edges of the object. This source distribution is qualitatively consistent with that expected from an expanding shock wave interacting with the interstellar gas (Oort, 1946). The strength of such an interaction must be nonuniformly distributed around the expanding surface in order to account for the observed intensity variations around the edge of the Loop. Preliminary calculations by Stevens (1972), show that a shock wave model appears quantitatively consistent with the data presented here. There is some correlation with the optical emission, but the correlation is not strong. Correlation with the 11-cm radio data of Kundu (1969) and the 6-cm map of Kundu and Becker (1972) shows only a weak similarity. A comprehensive comparison with the x-ray data of Gorenstein et al. (1971) is not possible, since the data presented in their report were not unfolded from their collimator response. Since the composite angular response function of their instrument was not given, we could not make a convolution of our data to determine whether it matched the results of Gorenstein et al. (1971) in detail. The general properties of the two observations are in reasonably good agreement, however. The total intensity in the 0.2 - 1.5 keV band is in good agreement with Gorenstein and coworkers (1971).

The observations of Borken et al. (1972) have been compared with the data of figure 2. The agreement is within the statistical accuracy of the data. Again, the overall flux reported by Borken and coworkers in the 0.1 - 1 keV band of $(1 \pm .2) \times 10^{-8}$ ergs/cm^2-sec agrees with the results obtained here.

Several features of the x-ray surface brightness show a conspicuous lack of correlation with either radio or optical emission and vice versa. The region below NGC 6992-5 in the southeast, which is a pronounced minimum in the radio map of Kundu (1969), and which shows very little H_α emission, is a surprisingly strong x-ray emitter. In this respect the x-rays suggest a more complete shell than either the radio or optical emission

The western half of the Loop shows a great deal of diffuse and filamentary visual structure. It is also a region of several relative maxima at radio wavelengths. However, in x-rays this region is much less intense than the eastern half of the Loop. The low x-ray intensity associated with NGC 6960 could be the result of greater interstellar gas absorption relative to the direction of NGC 6992-5. There is evidence for a dust lane just to the west (lower R.A.) of this filament as can be seen by a low density of stars on the 48-inch Schmidt Sky Survey plates. The gas associated with this dust could extend over into the direction of NGC 6960.

The radio and visual emission continues to the south in the form of a large arc. This is the region of the Loop which displays large radio polarization (Kundu 1969 ; Moffat, 1971; Kundu and Becker 1972). The direction of the polarization suggests that this arc is generated by material which has expanded out along the local magnetic field. The x-ray map does not rule out the possibility of emission from this arc but such emission must certainly be small. The only appreciable x-ray emission from the southern portion comes at a position which coincides well with the location of the relative maximum of unpolarized radio emission.

An unexpected bright region appears just to the east of the Loop's center. This element emits 8% of the total observed flux and is uncorrelated with any radio or optical feature. It is tempting to speculate that the stellar remnant of the supernova explosion is in this region and is responsible for this local maximum. The x-ray data presented here is suggestive, but further observations will be required to determine the nature of this bright region. The two bright regions at the north and northeast edges of the Loop may be interactions between local clouds of gas and the expanding shock wave. Such an interaction could possibly explain the bright region near the center of the Loop as well.

In view of the rather large intensity variation around the surface of the Cygnus Loop, it is reasonable to expect spectral variations. The statistical significance of the data presented in Table I is, however, inadequate to establish correlation between surface brightness and spectral shape, or between the shell geometry and the spatial distribution of the spectral ratio. If all the spectral ratio data in Table I are taken together and compared to the mean, a χ^2 of 16.5 is obtained for 17 degrees of freedom, implying that there is no excess fluctuation over random variations.

ACKNOWLEDGEMENTS

The authors wish to thank Dr. G. R. Riegler for useful discussions and for his substantial contributions to the development of the detector system. The Sounding Rocket Branch of the Goddard Space Flight Center and the White Sands Missile Range have generously contributed their support to this effort. Mr. P. Gloger contributed significantly to the development of the computer

program to generate the spatial map from the raw counting rate data. We also thank B. Baaqui, W. Moore, C. Sarazin, S. Speer and F. Yates of the California Institute of Technology for supporting the effort. Professor E. C. Stone made a valuable criticism of one point. This work was supported in part by the National Aeronautics and Space Administration grant NGR 05-002-219.

TABLE I

Percentage of Cygnus Loop X-ray Emission / Resolution Element

(Fraction of Resolution Element's Emission > 0.56 kev)

δ^* \ α^*	20^h56^m	20^h54^m	20^h52^m	20^h50^m	20^h48^m	20^h46^m
$32.^\circ0$	--†	5.2 (.79 ± .22)	1.4	12.1 (.44 ± .08)	5.8 (.65 ± .14)	--
$31.^\circ5$	3.7 (.30 ± .21)	8.6 (.48 ± .10)	2.9 (.65 ± .30)	4.6 (.76 ± .20)	3.7 (.42 ± .29)	1.8
$31.^\circ0$	4.3 (.58 ± .23)	1.5	8.3 (.73 ± .11)	0.3	-0.3	3.0 (.86 ± .66)
$30.^\circ5$	0.7	3.4 (.42 ± .39)	3.2 (1.0 ± .28)	-0.1	1.1	3.3 (.36 ± .25)
$30.^\circ0$	--	4.3 (.51 ± .20)	5.2 (.53 ± .19)	2.0	4.4 (.93 ± .23)	--
$29.^\circ5$	--	--		5.8 (.69 ± .14)	--	--

*α and δ in 1971.8 coordinates.

APPENDIX

The parameters of the detectors employed in the observations reported above are shown in Table II.

TABLE II

Detector Characteristics

Detector	Window Thickness Kimfol	Effective Area	FOV (FWHM)	Energy Band (keV)
A	270 $\mu gm/cm^2$	193 cm^2	$0.4^o \times 9.8^o$	0.25 - 1.5
B	270 $\mu gm/cm^2$	213 cm^2	$0.4^o \times 9.8^o$	0.15 - 1.5

The energy response of the detector system included two nominal energy bands (0.2 - 0.28 and 0.5 - 2.5 keV) with peak efficiencies of about 35 % in each band, set by the transmission of the Kimfol windows and the absorption of the methane gas at 150 torr pressure. The fan beam collimators of detectors A and B were oriented at 90 degrees with respect to each other so as to form an "X" response pattern in the sky. The orientation of this "X" is indicated in figure 1 as a function of time.

The mechanical collimators used for the mapping observations were constructed from etched stainless steel mesh. The meshes were stacked in a geometrical progression such that no transmission side lobes were present. The sharp edges of the grids eliminated the reflections that are sometimes found in mechanical slat collimators at energies near 1/4 keV. Twenty-five grids were used to obtain an 0.4^o full width at half maximum collimation (FWHM). The 9.8^o limit was determined by the window support collimator and not the mesh collimator. For a complete description of the mesh collimator construction see Stevens (1972).

The mathematical analysis used to determine the spatial structure of the Cygnus Loop from the observed counting rates during scanning is presented

below. For the region of sky near the Loop the celestial coordinates (α,δ) were transformed to a cartesian system (x,y), which for the region scanned is sufficiently accurate. The transmission as a function of the viewing angle of the collimators was measured prior to the flight using x-rays, yielding a transmission function $\eta^m(x',y')$, where m = A or B for the two detectors and x' and y' are the angular coordinates of directions in the collimator's frame of reference. The different low energy thresholds for counters A and B were taken into account by a modification of $\eta^A(x',y')$ in the form of a numerical factor determined from the spectrum of the Loop.

If $S(x,y)$ represents the intensity of x-rays emitted from the direction (x,y), then the number of photons entering the detector in the k^{th} one second time interval will be given by

$$F_k^m = \iint_{\Omega} \int_{k}^{k+1} S(x,y)\ \eta^m(x'[x,y],\ y'[x,y],\ t)\ dtdxdy$$

The smearing over angles caused by the motion of the collimator in the time interval Δt, serves to produce an effective collimator response broadened with respect to the collimator's stationary response by the extent of the motion during this interval. Let the modified response be $\eta_k^m(x',y')$, where the k subscript indicates the smeared response obtained during the k^{th} time interval. The source function was constructed in the form of discrete 0.5^o x 0.5^o cells, labelled S_{ij}. The effective collimator response was then folded with the 0.5^o cells. In this approximation the above integral becomes a sum

$$F_k^m = \sum_{ij} S_{ij}\ H_{ijk}^m$$

where k refers to the time index and H_{ijk}^m is the time and spatially averaged instrumental response which goes to zero outside the extent of $\eta_k^m(x',y')$. From the aspect solution and the instrumental angular response function, values of

H^m_{ijk} can be computed at each time k. The solution to the spatial distribution of S_{ij} proceeds by assuming values for S_{ij} and modifying these values in an iterative manner until the predicted values, f^m_k, agree with the observed values F^m_k. The initial values were all set to zero, represented by S^o_{ij}. For detector A the predicted value in the first interval is given by

$$f^A_1 = \sum_{ij} S^o_{ij} H^A_{ij1}.$$

Since S^o_{ij} was zero, f^A_1 did not agree with F^A_1. New trial source values S^1_{ij} were constructed in accord with the extent that they were sampled by H^A_{ij1}. The modification was given by

$$S^1_{ij} = S^o_{ij} + Q_1(F_1{}^A - f_1{}^A)H^A_{ij1}$$

where $Q_1 = [\sum_{ij} (H^A_{ij1})^2]^{-1}$ and the sums extend only over non-zero values of H^A_{ij1}.

The S^1_{ij} are the source values required to give the observed value F^A_1. These source values were then used to obtain a predicted value f^A_2. In a way entirely analogous to that given above, the values S^1_{ij} were modified to give agreement between the values f^A_2 and F^A_2. This gave the values S^2_{ij}. This process was continued through the 128 remaining one-second intervals of detector A and the source values S^{130}_{ij} were obtained. These served as the initial values for the beginning time interval of detector B. After iterating through the 130 one-second intervals of detector B, the values S^{260}_{ij} were obtained. These values were used as the initial values for the first time interval of detector A and the process was continued until the source values converged. These convergent values are labelled $\bar{S}_{ij}$.

The routine was tested on a trial source distribution consisting of a single source cell being non-zero and the rest zero. The expected values of f_k^m were generated for six scans across the source and then these f_k^m's were inverted by the above technique to arrive at the source values $\bar{S}_{ij}$. The $\bar{S}_{ij}$ matrix obtained reproduced the original function to within a small fractional error attributable to the inaccuracies involved in the integration scheme used to obtain the H_{ijk}^m . It should be noted that the iterative process outlined above requires a minimum of three scans to recover a point source.

There is clearly a question of convergence of the iterative process used to obtain the map in figure 2. The only check available at this time is a comparison between maps through the sequence of iterations. After twenty iterations the bright regions remain stable to within the statistical accuracy of the data. The patterns were examined for up to thirty iterations. The intensity variations between twenty and thirty iterations remained within the statistical precision obtained for each cell. It should be noted that the raw data provides a source detection at a 22-sigma level, whereas the data in figure 2 is only 16 sigma above background. The decrease in the sigma level is produced by the extra fluctuations introduced in the background by the iterative unfolding process. That extra noise must result from any unfolding process can be seen from the fact that the noise for a single observation is the result of all of the counts detected along the collimator response, whereas the noise on a single cell is the result of only a fraction of the counts detected from the full collimator sample in a given time interval.

REFERENCES

Borken, R., Doxey, R., and Rappaport, S. 1972 preprint.

Garmire, G. and Riegler, G. R. 1972, Astron. and Astrophysics, 21, 131.

Gorenstein, P., Harris, B., Gursky, H., Giacconi, R., Novick, R., Vanden Bout, P. 1971, Science, 172, 369.

Grader, R. J., Hill, R. W., Stoering, J. P. 1970, Ap. J. (Letters), 161, L45.

Henry, R. C., Fritz, G., Meekins, J. F., Friedman, H., Byram, E. T. 1968, Ap. J., 153, L11.

Kundu, M. R. 1969, Astrophys. J., 158, L103.

Kundu, M. R., and Becker, R. H. 1972, Astron. J., 77, 459.

Moffat, P. H. 1971, M.N.R.A.S., 153, 401.

Oort, J. H. 1946, M.N.R.A.S., 106, 159.

Stevens, J. C. 1972, Ph.D. Dissertation, California Institute of Technology.

FIGURE CAPTIONS

Fig. 1 - The counting rate versus time for detectors A and B, and the scan path of the detectors during the Cygnus Loop scan. Representative transits of the detectors over the edge of the Loop are numbered for reference to the scan plot. These transits are then drawn in and numbered on the scan plot to show the limits of the angular extent of the region of x-ray emission.

Fig. 2 - The x-ray intensity of the Cygnus Loop superimposed on a sketch of the H_α emission. Each bar represents approximately 10^{-10} ergs/(cm^{2}sec-0.25 deg^2)$^{-1}$ and two bars equal 1σ above the mean background. NGC 6992-5 is the lower part of the bright arch on the eastern boundary. NGC 6960 is on the western edge and NGC 6995 is just above NGC 6992.

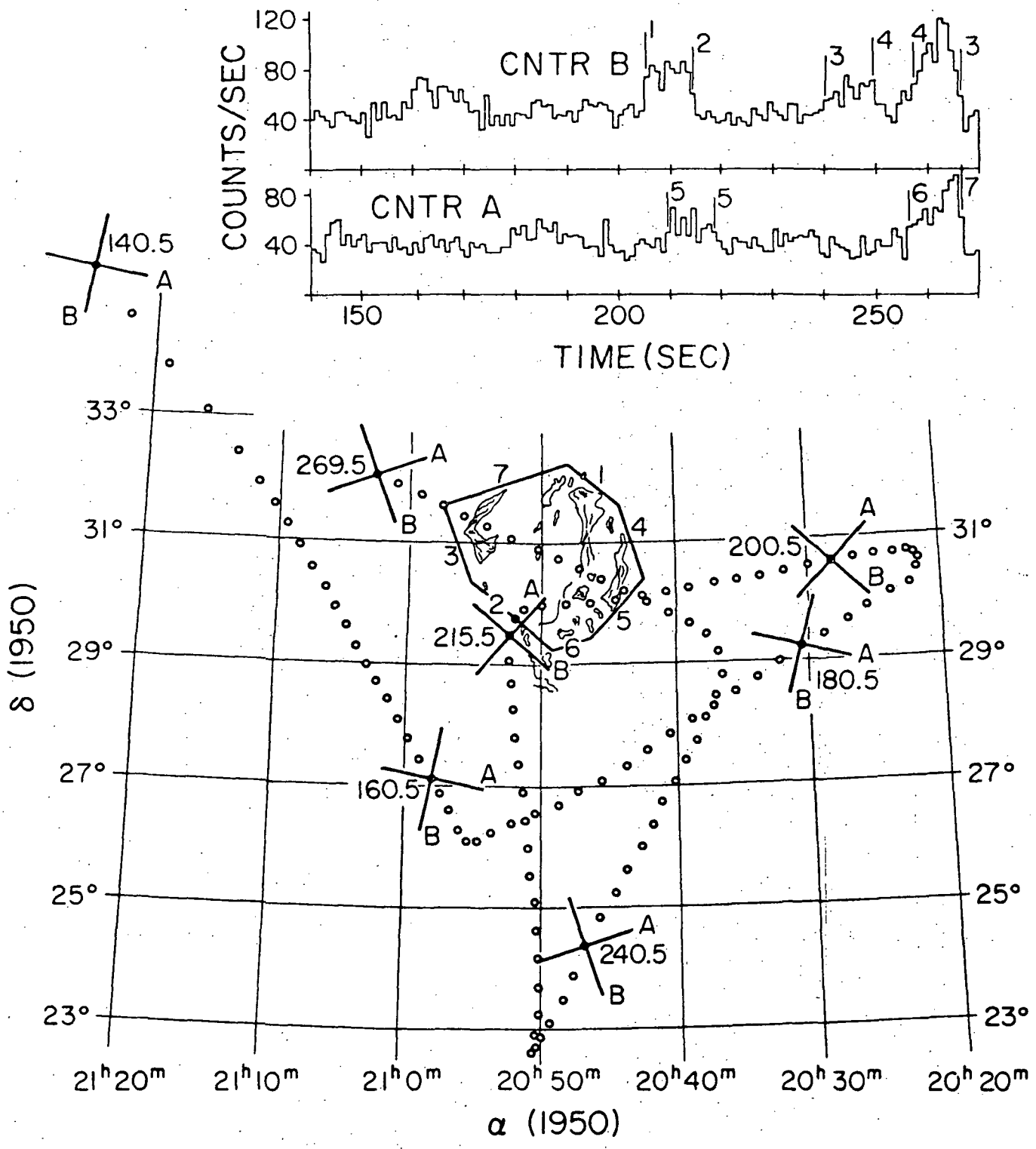
CNTR B
CNTR A
COUNTS/SEC
120
80
40
80
40
150
200
250
TIME (SEC)
140.5
269.5
215.5
160.5
240.5
200.5
180.5
A
B
33°
31°
29°
27°
25°
23°
δ (1950)
21h20m
21h10m
21h0m
20h50m
20h40m
20h30m
20h20m
α (1950)

Figure 1

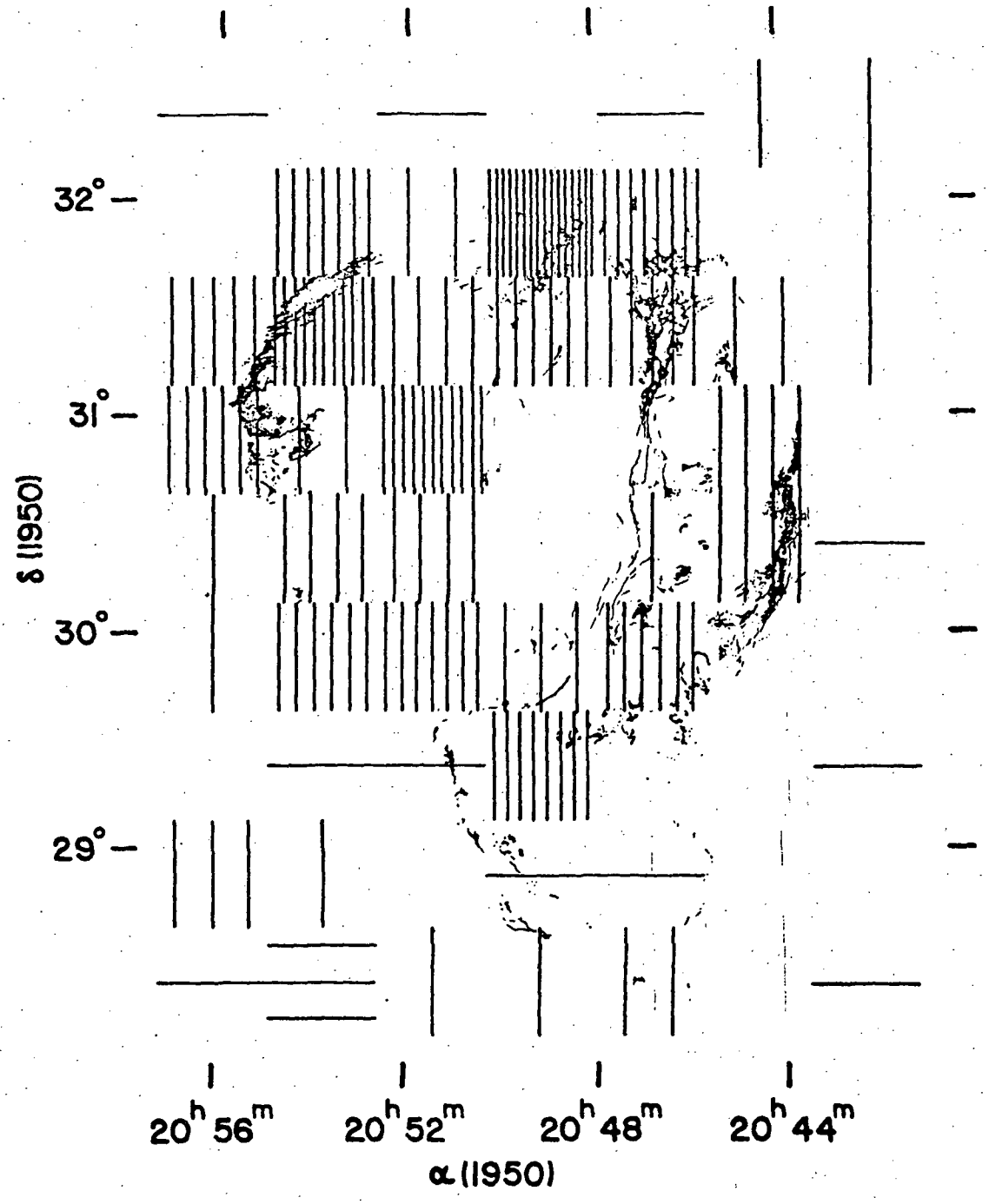

Figure 2

Observations of the He II 304 A and He I 584 A Nightglow

by

Guenter R. Riegler
Bendix Aerospace Systems Division
Ann Arbor, Michigan 48107

and

Gordon P. Garmire
California Institute of Technology
Pasadena, California 91109

ABSTRACT

An extreme ultraviolet telescope system was flown on an Aerobee 170 rocket while the sun was at a zenith angle of 133°. A set of aluminum, tin and parylene filters behind a grazing-incidence concentrator allowed unambiguous measurements of the atmospheric He II 304 A and He I 584 A radiation. The tin filter data at 177 km altitude result in a nightglow flux of I (584) = 4.4 R. The aluminum filter observations indicate a 304 A flux of 1.3 R at 180 km altitude.

An Aerobee 170 rocket was launched from the White Sands Missile Range, New Mexico, on 22 October 1971, 2145 MDT. In addition to other experiments, the rocket payload contained an extreme ultraviolet (EUV) detector system coupled with a paraboloidal reflecting concentrator. The purpose of this system was (1) to measure the 304 A and 584 A atmospheric nightglow, and (2) to search for discrete and diffuse sources of EUV radiation from beyond the solar system.

The following paragraphs will describe the detector system, the flight data, the search for discrete photon emitters, and the results relating to the He I and He II nightglow.

INSTRUMENTATION

A cross-section through the detector system is shown in Figure 1. Two concentric paraboloid mirrors focus a paraxial beam of light onto a point in the focal plane. This pair of mirrors acts as a photon collector without any true imaging properties but its effective collecting area is much larger than the detector cross-section itself. Compared to the usual geometry for EUV observation of the atmosphere, (see for example, Young, et. al., 1971) the present system has a significantly larger area-to-solid angle ratio and is therefore suitable for observations of point sources. The concentrators and baffles in this system also have the advantage of eliminating any direct photon and charged particle trajectories to the detector.

Pre-launch measurements at 584 A resulted in an effective collection area of 12.3 cm^2 and a field of view of 3.4×10^{-3} sr. The accuracy for both of these values is ±30% as estimated from comparisons of predicted and measured reflectivities and the repeatability of these measurements. Mirror reflectivities for other wavelengths were calculated by means of the reflection coefficients of Canfield et al. (1964) and Lukirskii et al. (1964).

The glancing angles of incidence for the two nested paraboloids vary from 9 deg to 18 deg. These glancing angles define a short wavelength cutoff near 75 A (Figure 2) which is needed to eliminate the counting rate contributions from known X-ray sources at shorter wavelengths.

The detector at the focal plane was a spiraltron photon multiplier with a 1 cm diameter entrance cone. The absolute detection efficiency was derived from a reference detector which had been calibrated against a windowless ionization chamber. The efficiency measurements are estimated to be accurate to within ±15% at wavelengths of 460, 584, 780, 906, 1216 and 1306A. The detection efficiency below 460 A follows measurements and data by Tohmatsu (1972, private communication).

A filter wheel was located in front of the focal plane. The six discrete positions of the wheel (tin, Parylene, a radioactive calibration source, Parylene, aluminum, and an opaque "solid" piece of metal)

changed every 8 s while the rocket was above 90 km altitude. Two positions contained a hydrocarbonate (Parylene N) film of 2860 A thickness, each consisting of two 1430 A thick layers in order to minimize pinhole leakage. The Parylene filter transmission was calculated from the sbsorption coefficients of Samson and Cairns (1965) and Henke et al. (1967). The combined efficiency of the mirror/Parylene/detector system is shown in Figure 2 by the curve marked "Parylene." If the bandwidth of this filter curve is defined by the wavelengths where the combined detection efficiency reaches 0.10 of the peak value, then we arrive at a band from 75 A to 230 A. The transmission of the 1600 A thick aluminum filter and the 1560 A thick tin filter were measured at 304, 416, 584, 780, 906, 1216, and 1306 A. Transmission characteristics at intermediate wavelengths were scaled appropriately from curves given by Hunter et al. (1966). The aluminum filter defined a band from 140A to 700A and was therefore sensitive to both the He II 304A and the He I 584A lines. The tin filter isolated the He I 584A line since it was sensitive only in the 500-800A range. A set of grids in front of the filter wheel rejects positively and negatively charged particles with energies up to approx. 20 eV which might reach the detector through pinholes or leakage paths around the filter wheel.

OBSERVATIONS

The trajectory of the EUV telescope axis on the attitude-controlled rocket is shown in Figure 3 in galactic coordinates, and in Figure 4 in

local polar coordinates. After initial maneuvers the experiment viewed the vicinity of the Cygnus Loop for approximately 120 s. A fast sweep at approximately 2°/s then moved the rocket orientation to the constellation Taurus where an intense emission of ≈ 50 A radiation had been reported by Hayakawa et al. (1971). Finally the field-of-view was oriented towards a region near the Seyfert galaxy NGC 1275 where it remained until the rocket re-entered the atmosphere. Further details are given by Stevens (1972).

The counting rate data are shown in Figure 5. The spiraltron electron multiplier is very sensitive to the residual pressure in its vicinity. Because of outgassing problems, no data were obtained until the rocket had reached an altitude of about 150 km. The initially high counting rates of the Parylene filter are therefore an indication of false counts which can be subtracted from the aluminum and tin filter data. The rates marked "solid" are an indication of the detector background rate.

Beyond a time after launch of T ≈ 180 s, the Parylene filter counting rate exceeds the counting rate for the solid wheel position by approximately 2 counts/s. A part of this rate difference can be accounted for by the effect of hydrogen Lyα radiation since an incident flux level of I (1216) = 7.5 kR (Young et al., 1971) results in a counting rate contribution from the hydrogen night glow of 0.7 count/s. On the other hand, pre-flight

laboratory measurements yield an upper limit to the 1216 A sensitivity which corresponds to an upper limit of 1.1 count/s for the Ly α contribution. The Parylene filter response to 304 A radiation may contribute up to 0.5 count/s between T = 200 s and 250 s, but this rate component disappears after T = 310 s. The contribution of other wavelengths between 170 A and 800 A must also be ruled out since the aluminum and/or tin filter would have transmitted an appropriate flux level after T = 310 s, contrary to observations (Figure 5). A possible contribution from the diffuse cosmic X-ray background will be discussed below.

The counting rate difference between the Parylene and solid metal filters may also be due to ambient charged particles. The area densities of the Parylene, aluminum and tin filters correspond roughly to the range of a 2 keV proton or alpha particle. Hill et al. (1970) observed charged particle fluxes of more than 100 particles/cm^2-s-sr at altitudes above h = 150 km and a magnetic shell parameter of L = 1.1. A comparison of the magnetic activity during the rocket flights of Hill et al. (1970) and the present observation indicates that a similar flux of low-energy electrons or other charged particles may have existed during this flight. In view of the absence of straight particle paths through the paraboloid concentrator structure it is difficult to estimate the resulting rate of charged particle events. At worst, the full counting rate difference of 2 counts/s could be

due to charged particles. In that case, the contribution to the aluminum and tin filter rates is of the same order since the range of charged particles in the metal filters is comparable to that in the Parylene filter.

EUV RADIATION FROM BEYOND THE SOLAR SYSTEM

Observations of discrete EUV emitters have been reported by a group at the University of California at Berkeley (C. S. Bowyer, private communication, 1972). The experiment described here did not scan the regions surveyed by the Berkeley group, so that a direct comparison is not possible.

The diffuse cosmic x-ray background. The Parylene filter observations correspond to the 75 A-230 A band where the diffuse cosmic x-ray background may still provide a significant flux contribution. Early low-energy x-ray observations, near 50 A, suggested an extragalactic origin of the diffuse background radiation with photoelectric absorption by the interstellar medium. A recent observation by Yentis et al. (1972) near 75 A resulted in a spectrum for the diffuse cosmic x-ray background which exhibits a steep increase in flux level towards longer wavelengths. If this spectrum continues to 150 A without interstellar absorption, then it contributes 1.4 counts/s to the counting rate observed through the Parylene filters (as discussed in the preceding section, the H Lyα flux contributes from 0.7 to 1.1 counts/s to the Parylene filter rate). A

photo-absorption cutoff near 150 A occurs within a column density of $\int n_H \cdot ds \approx 1.8 \times 10^{19}$ cm^{-2}; even if the interstellar gas density is assumed to be as low as 0.1 H atom/cm^2, this cutoff implies that the observed low-energy x-ray background is generated within a distance of approximately 60 pc from the sun. The Parylene filter observations can therefore be used as a constraint on the wavelength band in which the spectrum suggested by Yentis et al (1972) remains valid.

The EUV observations with the Parylene filter, centered on approximately 120 A, can also be interpreted in terms of the defunct-pulsar model of Ostriker et al. (1970). This model assumes that old pulsars, or neutron stars, should accrete interstellar matter and emit black-body radiation which peaks near 120 A (100 eV). If there are 10^9 neutron stars in the galactic disc, each emitting 10^{31} - 10^{32} ergs/s, and a photon mean free path of 100 pc is assumed, then the assumptions of Ostriker et al (1970) predict a 120 A flux between 540 photons/cm^2-s-sr and 5400 photons/cm^2-s-sr. The upper range of the flux level prediction can be ruled out since the full Parylene/solid metal counting rate difference of 2 counts/s corresponds to an 120 A flux of 1200 photons/cm^2-s-sr.

Existence of discrete EUV sources. Figure 6 shows counting rates in 1-second intervals after subtraction of a smoothly varying background given by the "solid" cover data. The rates are statistically consistent

with a slowly varying diffuse EUV radiation except near T = 242 s and T = 273 s. With a field of view of 3.8°diameter and a scan rate of 0.5°/s at 242 s, a point source along the scan path would generate a counting rate pattern of 7.6 s full width at half maximum. Although an off-axis traversal might be involved, we consider it unlikely that the observed feature was caused by a discrete point-like EUV source. Instrumental effects may also be ruled out because of the absence of comparable counting rate fluctuations for any filter wheel position after T ≈ 310 s.

The telescope scan rate at T = 273 s was 1.9°/s so that the full width at half maximum response to a point source would be $\leq$ 2 s. If the feature at T = 273 s is due to a discrete source along the scan path (RA = 21^h20^m, $\delta = +33^\circ.1$) then its flux level corresponds to I (500 - 800A) ≈ 300 photons/cm^2 - s. There is no prominent candidate object within the error box of the present observations. In summary, the causes for the features at 242 s and 273 s are not understood, although a point-source explanation may be invoked for the latter observation.

Intense emission of ≈ 50 A radiation was reported by Hayakawa et al. (1971) to originate in a region of the constellation Taurus which was scanned by the present experiment. Although their data do not permit a determination of the source spectrum, Hayakawa and co-workers find that their measurements are consistent with an exponential spectrum of

equivalent temperature between 0.3 and 0.5 keV. Even if the source were located within 150 pc from the earth, the 120 A flux would have generated a signal of only one or two standard deviations above the Parylene filter counting rate after T = 320 s. We can therefore only state that the spectrum of the hypothetical source is not significantly steeper, i.e. softer, than the spectral shape quoted by Hayakawa et al. (1971).

OBSERVATIONS OF THE EUV NIGHTGLOW

The remainder of the discussion will concern observations of the He II 304A and He I 584A nightglow.

A contamination of the aluminum and tin filter data with H Ly α and β radiation can be ruled out for the following reasons: (1) Laboratory measurements of the filter transmission and detector sensitivity prior to flight gave upper limits to the overall H Ly α and β sensitivity. For example, the sensitivity ratio for the aluminum filter system is η (1216 A)/η (304 A) $< 10^{-5}$. (2) An important feature of the results are the data from the aluminum and tin filters after T = 320 s. At this time the rocket was below 140 km and the telescope viewed an area near the anti-solar direction (see Figure 4). However, the hydrogen Ly α 1216 A flux is still quite strong at altitudes above approximately 100 km and the counting rates observed are consistent with the detector background. We can therefore state that the 1216 A contribution to the aluminum and tin filter data was probably negligible.

The possibility of O^{++} 304 A emission was suggested by Carlson (1972). At altitudes below 700 km the O^{++} and He^{+} densities are comparable so that the oxygen 303.799 A transition may contribute up to 13% of the helium 303.782 A resonance line intensity. However, at altitudes between 2200 and 3000 km the O^{++} density is approximately two orders of magnitude lower than the He^{+} density (J. Hoffman, private communication, 1973). The shadow height during the present observations, calculated for an assumed cutoff of solar 304 A radiation at an altitude of 200 km at the terminator, was never less than approximately 1800 km. The oxygen transition contribution to the scattered solar 304 A radiation can therefore be assumed to be negligible.

The net aluminum and tin filter counting rates were obtained by subtracting from the observed rates an average counting rate for the Parylene and "solid" filter positions. Figure 6 shows the resulting net rates in 1-second intervals.

584 A Observations. The tin filter data were compared to a model of atmospheric nightglow radiation. Alternative interplanetary models (Meier and Weller, 1972; Bowyer et al., 1973) will not be considered here since the present experiment included only a small number of viewing directions and therefore does not permit a distinction between the models.

In fact, the data-fitting procedure discussed below remains valid whether the radiation incident above h_o=250 km is a result of scattering in the earth's atmosphere or by interplanetary matter. Since the viewing direction is approximately constant up to 265 s after launch, the expected counting rate dependence is determined by atmospheric attenuation as a function of rocket altitude. The absorption cross sections for N_2, O_2 and O were adopted from Samson and Cairns (1964) and Cairns and Samson (1965). The T = 900°C model atmosphere by Jacchia (1970) was used for the 584 A and the subsequent 304 A calculations. The reference altitude h_o = 250 km was chosen since absorption of both 304 A and 584 A radiation above this height becomes negligible, and the attenuation and source intensity calculations can therefore be separated.

The model curve for 584 A radiation prior to T = 265 s is given by atmospheric attenuation of a constant flux level incident at h_o. After T = 265 s, the flux level at h_o was varied as a function of zenith and azimuth angle in proportion to the scattered solar 584 A flux from an optically thick spherical shell atmosphere (R. R. Meier, private communication, 1972; Meier and Weller, 1972). The complete model curve was scaled in absolute intensity by a least-squares fit to the tin filter data. The resulting counting rate distribution is shown as the lower curve in Figure 6. It must be pointed out that the model curve after T ≈ 280 s is rather sensitive

to the coefficients used in the atmospheric attenuation calculation, and, to a lesser degree, to the zenith-angle dependence of the radiation incident at h_o. The 584 A curve in Figure 6 corresponds to an intensity of $I(584, h_o) = 11.4$ R (1 R is equivalent to 8×10^4 photons/cm^2-s-sr) incident at a zenith angle z = 25° and azimuth angle a = 272°. The tin filter counting rate observed at T = 225 s corresponds to I (584, 180 km) = 4.4 R. This observed value is considerably larger than the expected flux from a spherical, optically thick atmosphere (Meier and Weller, 1972) unless an unreasonably narrow solar 584 A line is assumed. The observations therefore suggest an interplanetary or interstellar origin of the 584 A emission, but the number of viewing directions in the present survey is too small to permit a more detailed definition of the radiation source.

304 A Observations. The detection sensitivities (Figure 2) of the aluminum and tin filter observations to 584 A radiation are identical, so that the tin filter counting rates can be subtracted from the aluminum filter counting rates to obtain the net 304 A response. Since the filter wheel requires a time shift between aluminum and tin filter observations, the 584 A model curve was used to subtract the interpolated 584 A contribution from the aluminum filter data. A model for the 304 A response was fitted in absolute intensity by a least-squares procedure to the

resulting "net 304 A counting rate." This model includes the atmospheric attenuation of 304 A radiation from h_o to altitude h under zenith angle z, and the relative emission incident at h_o as a function of viewing direction.

The distribution of helium ions is determined by photoionization and charge exchange as well as by diffusion, solar activity, and other effects which are intimately linked to geomagnetic activity. From magnetic-latitude surveys it was found that the He^+ density drops sharply near the polar regions at magnetic latitudes corresponding to L-parameters between 3 and 5. The relative emission intensity of scattered solar 304 A radiation was therefore calculated for a single-scattering, constant-density plasmaspheric He^+ model which has been used by Meier and Weller (1972) and Paresce et al. (1972) to fit experimental data. In this model, the intensity of scattered solar 304 A radiation is set proportional to the linear path length difference between the shadow height and a sharp L-shell cutoff at the boundary of the plasmasphere. The proportionality constant includes an increase in the He^+ density by a factor of 1.5 for magnetic latitudes changing from 30° to 50° (J. Hoffman, quoted by Meier and Weller, 1972.) Other effects, like the departure from isotropic scattering and absorption within the scattering helium ion column, have a negligible influence on the model fit for the viewing sequence discussed here.

The upper end of the scattering column was assumed to have a sharp cutoff at a magnetic dipole shell parameter of L = 4. This L-value was adopted from the model calculations by Meier and Weller (1972) and Paresce et al. (1972) who used L = 4 and L = 4.25, respectively. Binsack's (1967) statistical relation between the L-value of the magnetospheric boundary and the K_p index during the 6-hour period prior to launch would actually predict a magnetic shell parameter L = 5.4. Because of the large spatial and temporal separation of 304 A measurements with the aluminum filter, the present observations do not permit a determination of the L-value from the experimental results. However, in view of the variations in altitude and pointing direction between T = 265 s and T = 310 s, a change in the L-shell cutoff value has a weak effect on the counting rate prediction for the 304 A observation. An increase from L = 4 to L = 5.4 increases the predicted counting rate at T = 288 s by 14 counts/s (compare Figure 6) and would give a somewhat poorer fit to the data than the L = 4 curve.

The best-fitting 304 A model curve corresponds to a flux level of I (304, h_o) = 2 R. The contribution of 304 A radiation to the aluminum filter response at T = 240 s is equivalent to I (304, 177 km) = 1.3 R.

The sum of the 304 A model curve and the 584 A curve yields the combined aluminum filter curve shown in Figure 6.

Comparison with Results by Other Observers. At altitudes from 207 km to 217 km and almost identical solar-terrestrial configuration, Young et al. (1971) measure 5.3 R for the 304 A flux at the same solar aspect angle. Considering the possible systematic errors in the area and solid angle calibrations, the two sets of results are found to be in reasonable agreement. A more recent observation by Paresce et al. (1972) also results in a He II flux value of I (304, 250 km) = (3-5) R. Measurements by Ogawa and Tohmatsu (1971) are in qualitative agreement with the results reported here, but a detailed comparison is more difficult.

A discrepancy exists between the present measurement of the 584 A flux and an upper limit of approximately 4 R deduced from the report of Young et al. (1971). Our measurement is, however, in good agreement with other recent positive observations of 584 A radiation (Bowyer et al., 1973; Meier, private communication, 1973).

SUMMARY

An EUV telescope system was used to observe portions of the night sky from rocket altitudes. The system, consisting of grazing incidence concentrators, particle rejection grids, absorption filters and a spiraltron detector, was designed to minimize charged particle and long-

wavelength radiation effects. The combination of aluminum and tin filters permits a separation of the 304 A and 584 A radiation.

There is no clear evidence for the observation of point-like sources of EUV radiation, although anomalous counting rate fluctuations occurred at certain times during the flight.

The counting rate difference between the Parylene filter and the solid wheel positions can be used to place an upper limit to the ≈ 120 A component of the diffuse cosmic x-ray background. We show that the x-ray background spectrum suggested by Yentis et al. (1972) cannot continue to wavelengths longer than approx. 150 A.

The tin filter observations are best fitted by a 584 A attenuation curve which results in I (584) = 4.4 R at h = 180 km. From the aluminum and tin filter data we deduce a He II 304 A nightglow flux of I (304) = 1.3 R at an altitude of 177 km.

ACKNOWLEDGEMENTS

We are grateful to Dr. R. Meier of the Naval Research Laboratory for supplying the 584 A scattering calculations and model computations for the 304 A nightglow contribution. The authors wish to thank Dr. J. Stevens for his support during the launch preparations and the aspect determination. The Sounding Rocket Branch of the Goddard Space Flight Center and the White Sands Missile Range have generously contributed their supports to this effort. We also thank B. Baaqui, P. Gloger, C. Sarazin, S. Speer and F. Yates of the California Institute of Technology, and R. Bird and K. More of the Bendix Corporation, for their help on this project. This work was supported in part by the National Aeronautics and Space Administration grants NGL 05-002-007 and [redacted]. NGR 05-002-219

REFERENCES

Bowyer, S., F. Paresce, and S. Kumar, Evidence for an interplanetary source of diffuse He I, 584 A radiation, Bull. Am. Astron. Soc., 5, 37, 1963.

Cairns, R.B., and J.A.R. Samson, Total absorption cross section of atomic oxygen below 910 A, Phys. Rev., 139, A1430, 1965.

Canfield, L.R., G. Haas, and W.R. Hunter, The optical properties of evaporated gold in the vacuum ultraviolet from 300 A to 2000 A, J. de physique, 25, 124, 1964.

Carlson, R.W., Possibility of O III 304-A emissions in the extreme ultraviolet airglow, J. Geophys. Res., 77, 6282, 1972.

Hayakawa, S., T. Kato, T. Kohmo, K. Nishimura, Y. Tanaka and K. Yamashita, New soft X-ray source in the Aries-Taurus region, Nature, 231, 76, 1971.

Hill, R.W., R.J. Grader, F.D. Seward, and J.P. Stoerling, Soft particle flux above 130 km at mid-latitude, J. Geophys. Res., 75, 7276, 1970.

Henke, B.L., R.L. Elgin, R.E. Lent, and R.B. Ledingham, X-ray absorption in the 2 - 200 A region. Norelco Reporter, 14, 112, 1967.

Hunter, W.R., D.W. Angel, and R. Tousey, Thin films and their uses for the extreme ultraviolet, Appl. Optics, 4, 891, 1965.

Jacchia, L.G., New static models of the thermosphere and exosphere with empirical temperature profiles, Smithsonian Astrophysical Observatory Special Report, 313, 1970.

Lukirskii, A.P., E.P. Savinov, O.A. Ershov and Yu. F. Shepelev, Reflection coefficients of radiation in the wavelength range from 23.6 to 113 A for a number of elements and substances and the determination of the refractive index and absorption coefficients Optics and Spectroscopy, 16, 168, 1964.

Meier, R.R. and C.S. Weller, EUV resonance radiation from helium atoms and ions in the geocorona, J. Geophys. Res., 77, 1190, 1972.

Ogawa, T. and T. Tohmatsu, Sounding Rocket Observations of Helium 304- and 584-A Glow, J. Geophys. Res., 76, 6136, 1971.

Ostriker, J.P., M.J. Rees, and J. Silk, Some observable consequences of accretion by defunct pulsars, Astrophys. Letters, 6, 179, 1970.

Paresce, F., S. Bowyer and S. Kumar, Observations of the He II, 304 A radiation in the night sky, J. Geophys. Res., (to be published) 1972.

Samson, J.A.R., and R.B. Cairns, Absorption and photoionization cross sections of O_2 and N_2 at intense solar emission lines, J. Geophys. Res., 69, 4538, 1964.

Samson, J.A.R., and R.B. Cairns, A carbon film-scintillator combination suitable for the selective detection of radiation in the extreme ultraviolet, Appl. Optics, 4, 915, 1965.

Stevens, J.S., Soft X-rays from the Cygnus Loop, unpublished doctoral thesis, California Institute of Technology, 1972.

Yentis, D.J., R. Novick, and P. Vanden Bout, Galactic-latitude dependence of low-energy diffuse x-rays, Ap. J., 177, 365, 1972.

Young, J.M., C.S. Weller, C.Y. Johnson, and J.C. Holmes, Rocket observations of the far UV nightglow at Lyman α and shorter wavelengths, J. Geophys. Res., 76, 3710, 1961.

FIGURES

Figure 1. Cross section through the detector system.

Figure 2. Detection efficiency of the concentrator/filter/detector system as a function of wavelength.

Figure 3. Trajectory of the extreme ultraviolet telescope axis in galactic coordinates.

Figure 4. Trajectory of the extreme ultraviolet telescope axis in local polar coordinates.

Figure 5. Observed counting rate as function of time. The heights of the vertical bars or of the diamonds correspond to the one standard deviation errors.

Figure 6. Net aluminum and tin filter counting rates. The solid lines represent the best-fitting 304 A and 584 A model curves, including zenith angle dependence and atmospheric attenuation (see text). The tin filter counting rate at 225 s (180 km altitude) corresponds to I(584 A) = 4.4 R. The observed aluminum filter counting rate at 240 s (177 km) represents the combined response to I (584 A) = 4.1 R and I(304 A) = 1.3 R.

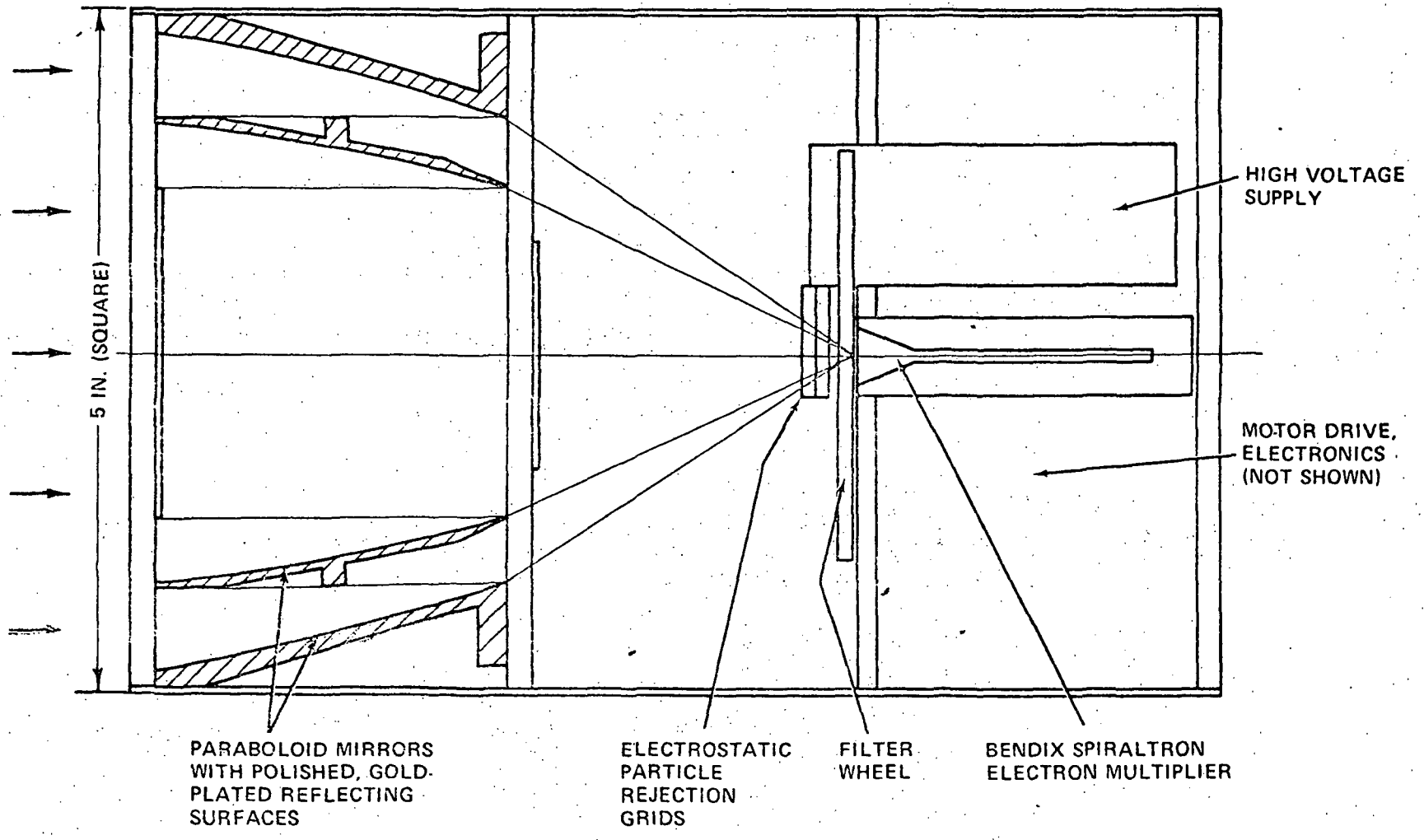
5 IN. (SQUARE)
HIGH VOLTAGE SUPPLY
MOTOR DRIVE, ELECTRONICS (NOT SHOWN)
PARABOLOID MIRRORS WITH POLISHED, GOLD-PLATED REFLECTING SURFACES
ELECTROSTATIC PARTICLE REJECTION GRIDS
FILTER WHEEL
BENDIX SPIRALTRON ELECTRON MULTIPLIER

FIGURE 1

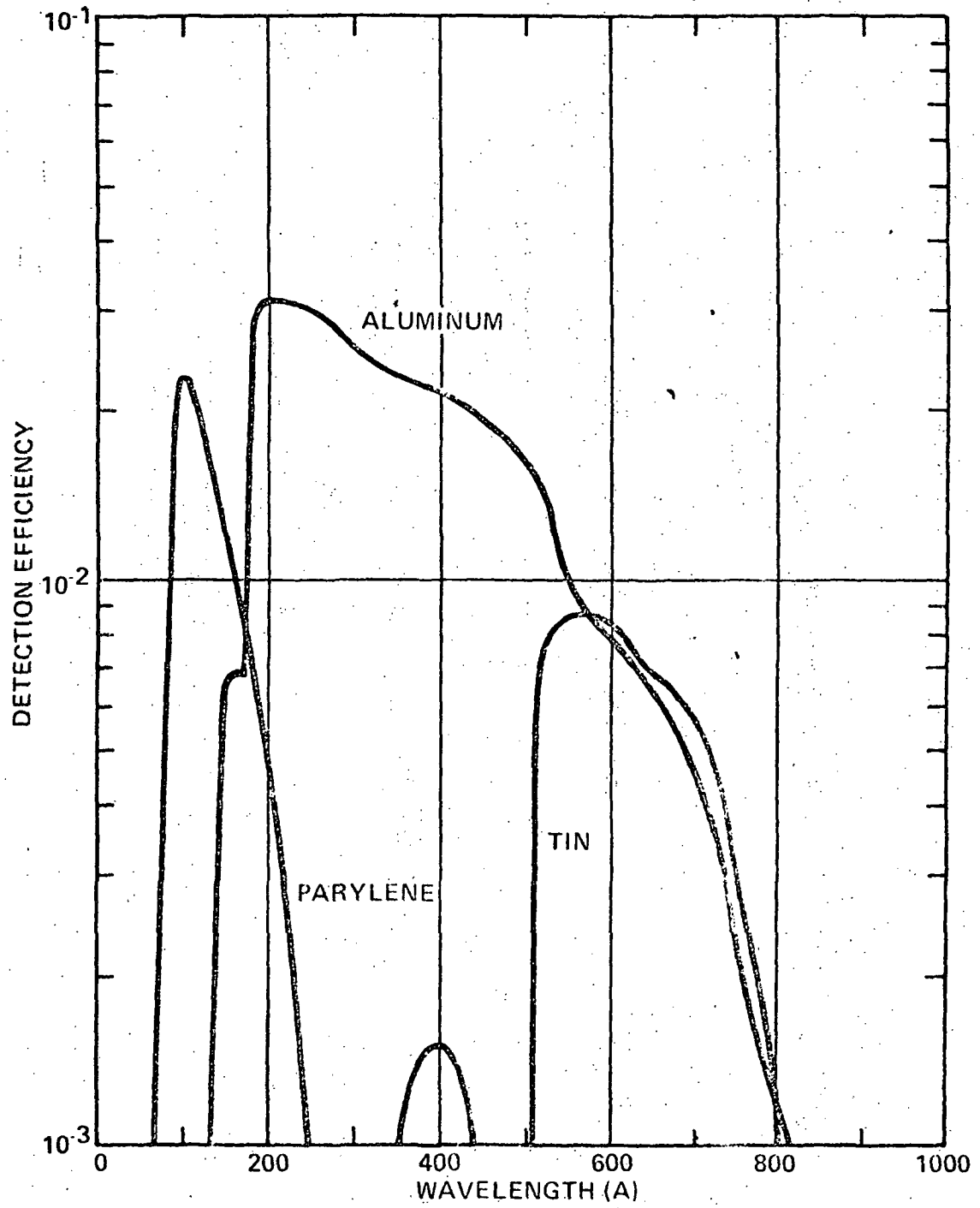
10^{-1}
10^{-2}
10^{-3}
DETECTION EFFICIENCY
ALUMINUM
PARYLENE
TIN
0
200
400
600
800
1000
WAVELENGTH (A)

FIGURE 2

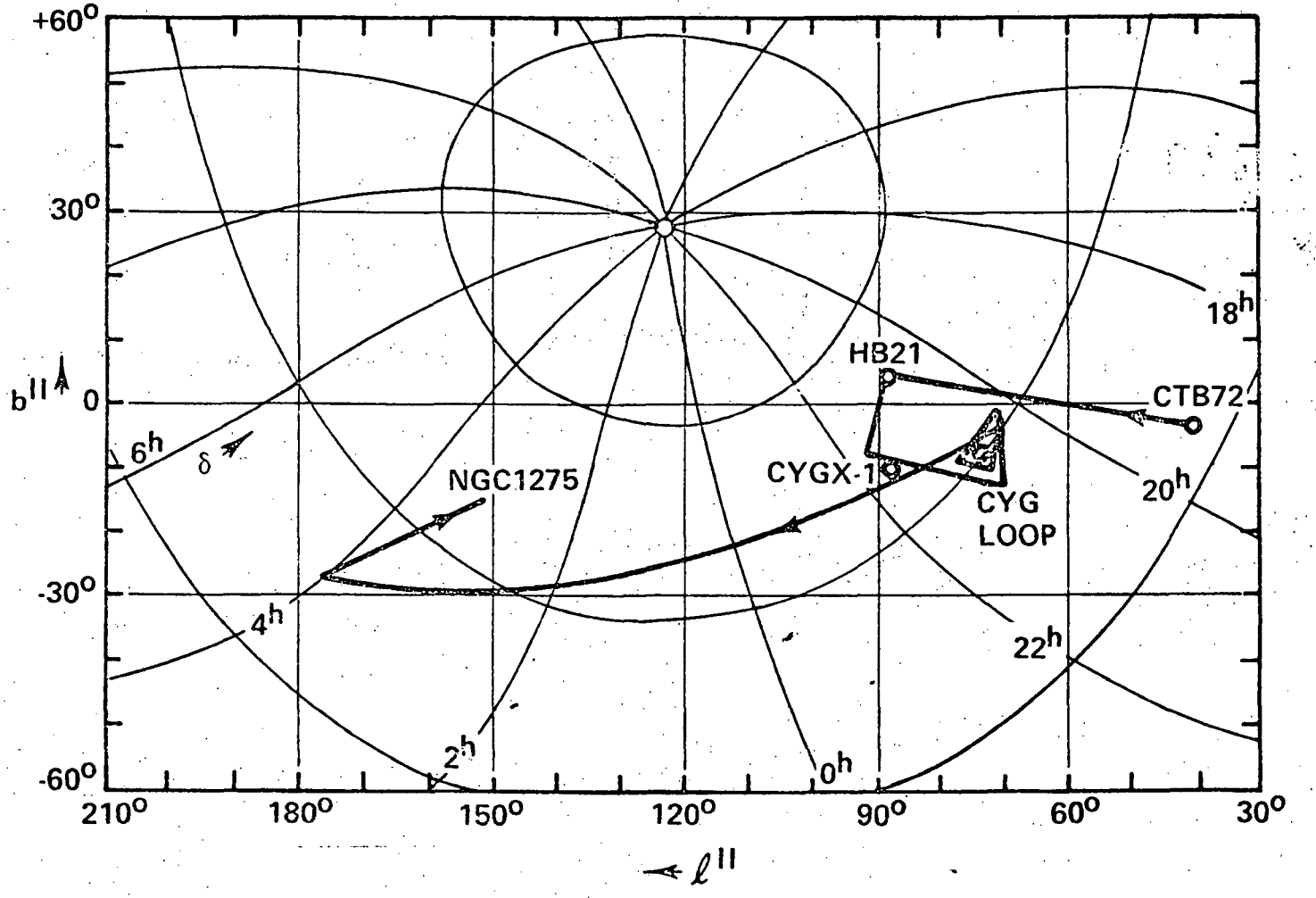
+60°
30°
0
-30°
-60°
b^{II}
210°
180°
150°
120°
90°
60°
30°
ℓ^{II}
18^h
20^h
22^h
0^h
2^h
4^h
6^h
δ
HB21
CTB72
CYGX-1
CYG
LOOP
NGC1275

FIGURE 3

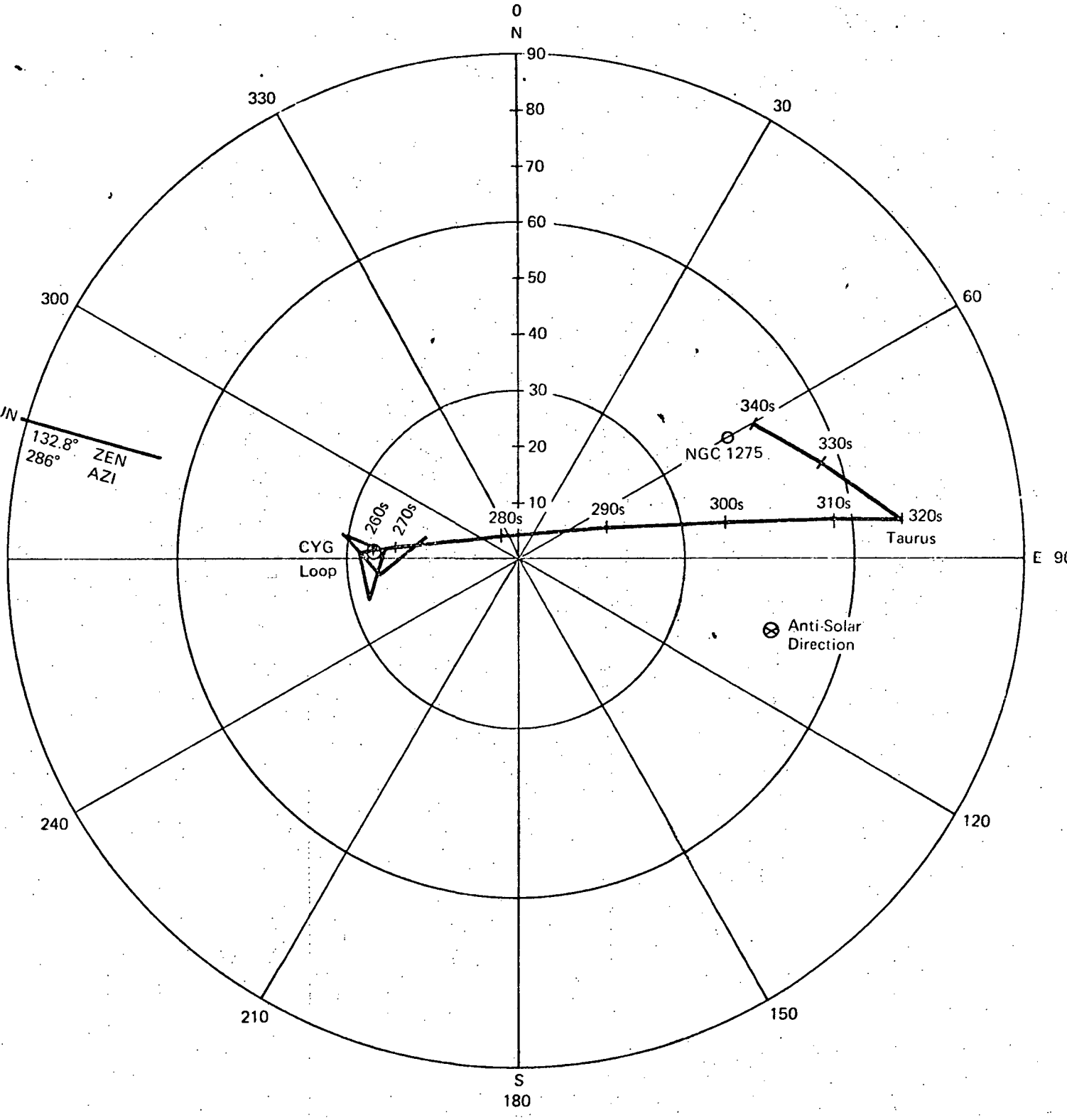
0
N
90
80
70
60
50
40
30
20
10
30
60
120
150
S
180
210
240
300
330
132.8°
286°
ZEN
AZI
280s
290s
300s
310s
320s
330s
340s
Taurus
NGC 1275
260s
270s
CYG
Loop
Anti-Solar
Direction

FIGURE 4

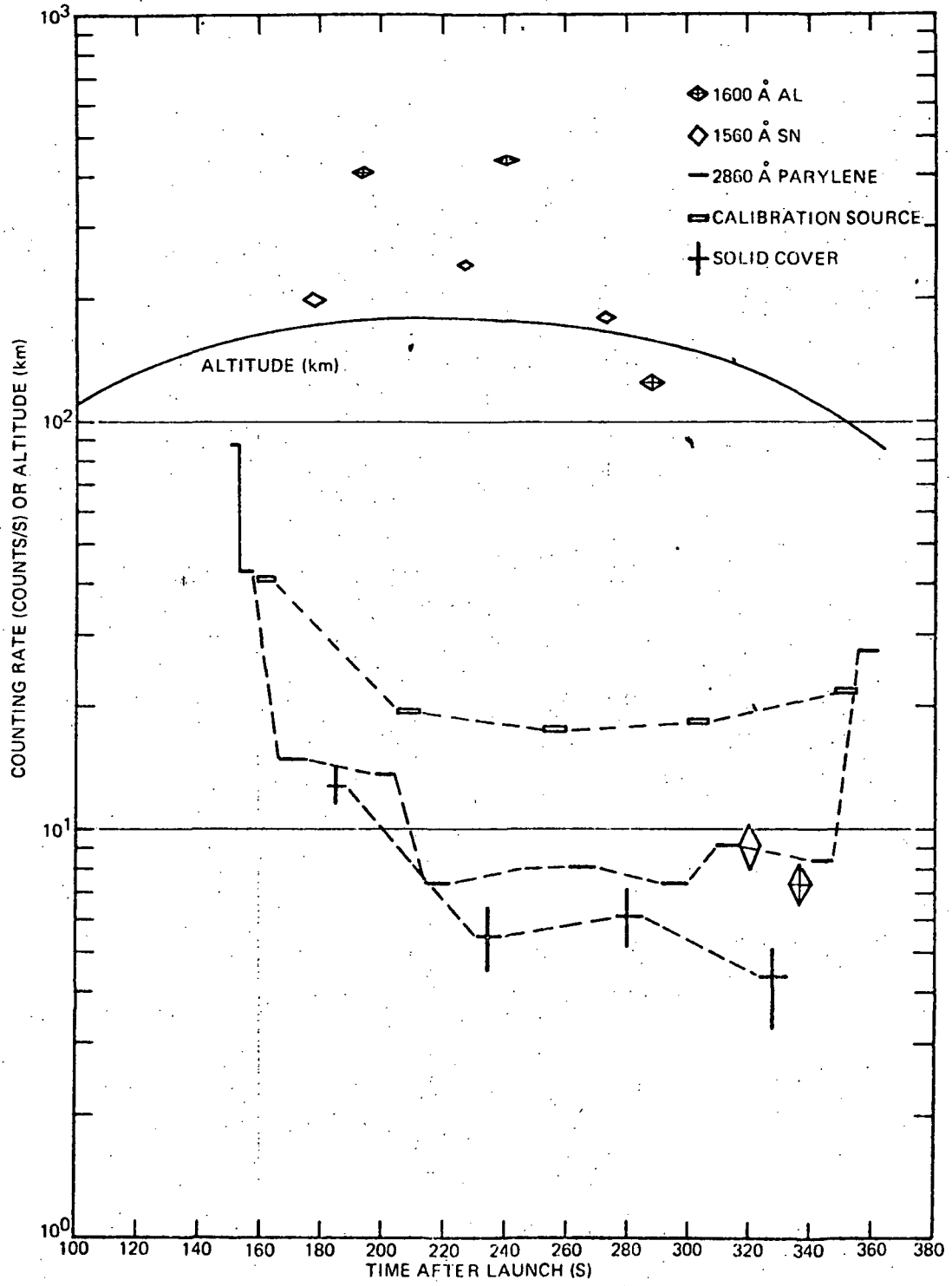
1600 Å AL
1560 Å SN
2860 Å PARYLENE
CALIBRATION SOURCE
SOLID COVER
ALTITUDE (km)
COUNTING RATE (COUNTS/S) OR ALTITUDE (km)
TIME AFTER LAUNCH (S)
10^3
10^2
10^1
10^0
100
120
140
160
180
200
220
240
260
280
300
320
340
360
380

FIGURE 5

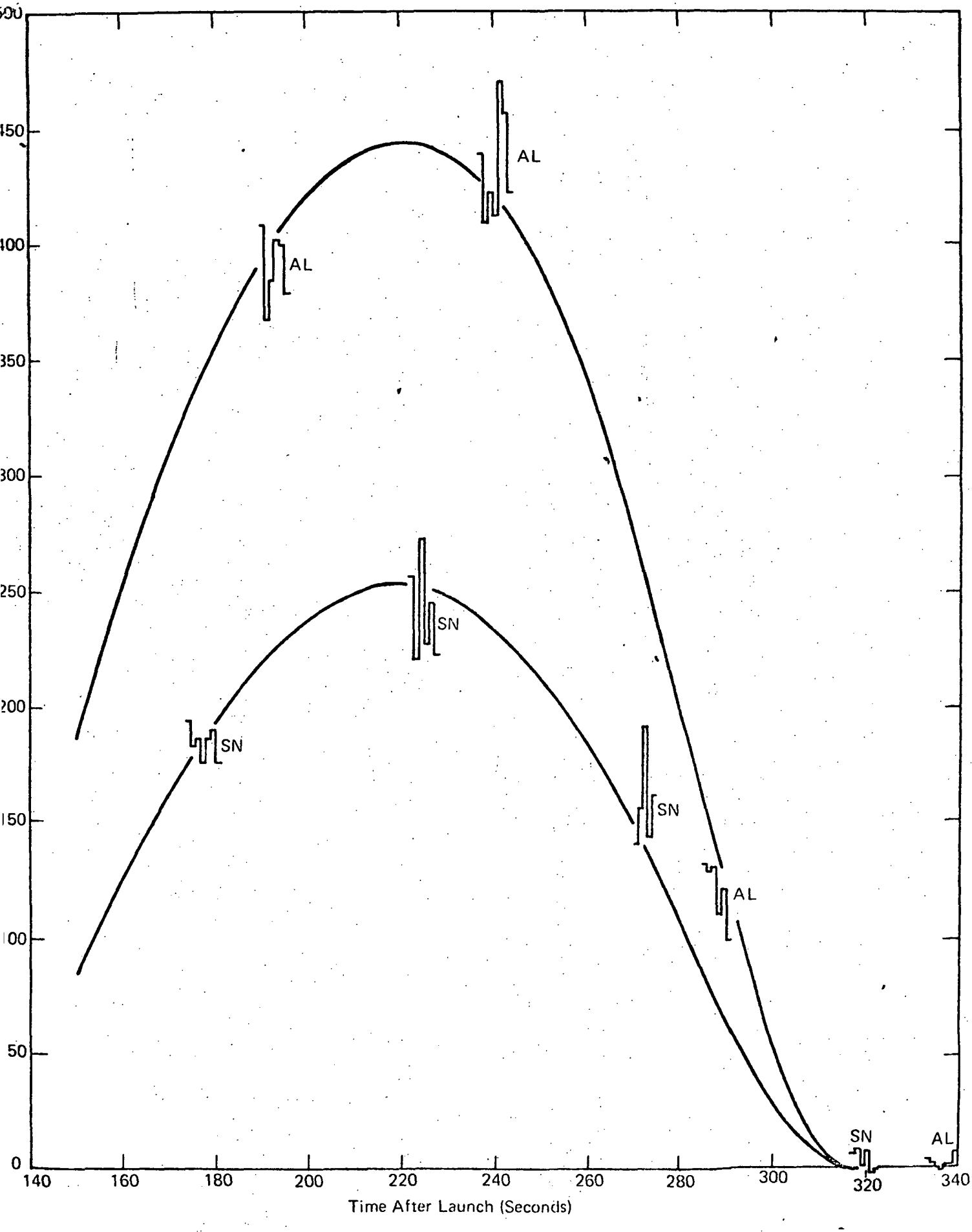
AL
AL
SN
SN
SN
AL
SN
AL
0
50
100
150
200
250
300
350
400
450
500
140
160
180
200
220
240
260
280
300
320
340
Time After Launch (Seconds)